

Symplecticity-Preserving Prediction of Hamiltonian Dynamics by Generalized Kernel Interpolation

Robin Herkert ^{*1}, Tobias Ehring ^{†2}, and Bernard Haasdonk^{‡3}

^{1,2,3}Institute of Applied Analysis and Numerical Simulation, University of Stuttgart, Pfaffenwaldring 57, 70569 Stuttgart, Baden-Württemberg, Germany

Abstract

In this work, a kernel-based surrogate for integrating Hamiltonian dynamics that is symplectic by construction and tailored to large prediction horizons is proposed. The method learns a scalar potential whose gradient enters a symplectic-Euler update, yielding a discrete flow map that exactly preserves the canonical symplectic structure. Training is formulated as a gradient Hermite–Birkhoff interpolation problem in a reproducing kernel Hilbert space, providing a systematic framework for existence, uniqueness, and error control. Algorithmically, the symplectic kernel predictor is combined with structure-preserving model order reduction, enabling efficient treatment of high-dimensional discretized PDEs. Numerical tests for a pendulum, a nonlinear spring–mass chain, and a semi-discrete wave equation show nearly algebraic greedy convergence and long-time trajectory errors reduce by two to three orders of magnitude compared to an implicit midpoint baseline at the same macro time step.

Keywords: Kernel methods, Greedy methods, Hamiltonian system, Symplectic integrator

1 Introduction

Many conservative physical phenomena, for instance in classical mechanics, theoretical chemistry, or molecular dynamics, can be formulated as Hamiltonian systems, whose mathematical structure encode the conservation of energy. In canonical coordinates $x = (q, p)^\top \in \mathbb{R}^{2n}$, $n \in \mathbb{N}$ and for $t \in I := [0, T] \subset \mathbb{R}$, the dynamics associated with a Hamiltonian function $\mathcal{H} \in C^1(\mathbb{R}^{2n}, \mathbb{R})$ are given by

$$\dot{x}(t; x_0) = J_{2n} \nabla \mathcal{H}(x(t; x_0)), \quad x(0; x_0) = x_0, \quad (1)$$

where

$$J_{2n} := \begin{bmatrix} 0_n & I_n \\ -I_n & 0_n \end{bmatrix}$$

is the canonical Poisson matrix, and $0_n, I_n \in \mathbb{R}^{n \times n}$ denote the zero and identity matrices of size n , respectively. For each initial value $x_0 \in \mathbb{R}^{2n}$, we denote by $x(t; x_0)$ the solution of the Hamiltonian system (1) at time $t \in I$. As a standing example throughout this work, we consider for $n = 1$ the mathematical pendulum, which is governed by the Hamiltonian

$$\mathcal{H}(q, p) = \frac{p^2}{2ml^2} + mgl(1 - \cos q),$$

^{*}robin.herkert@ians.uni-stuttgart.de

[†]tobias.ehring@ians.uni-stuttgart.de

[‡]haasdonk@ians.uni-stuttgart.de

and the corresponding equations of motion

$$\dot{q}(t) = \frac{p(t)}{ml^2}, \quad \dot{p}(t) = -mgl \sin(q(t)),$$

where q denotes the angular displacement, p the angular momentum, m the mass, l the pendulum length, and g the gravitational acceleration.

Several properties follow from the Hamiltonian structure. In particular, the Hamiltonian is conserved along trajectories,

$$\mathcal{H}(x(t; x_0)) = \mathcal{H}(x_0) \quad \text{for all } t \geq 0,$$

and the associated flow map $\Phi^t : \mathbb{R}^{2n} \rightarrow \mathbb{R}^{2n}$, defined by

$$\Phi^t(x_0) := x(t; x_0),$$

is symplectic. Here a differentiable map $\Psi : \mathbb{R}^{2n} \rightarrow \mathbb{R}^{2n}$ with Jacobian $D\Psi$ is called symplectic if

$$(D\Psi(x))^\top J_{2n} D\Psi(x) = J_{2n} \quad \text{for all } x \in \mathbb{R}^{2n}.$$

Note that, in the following, we omit the dependence of the solution $x(t; x_0)$ on the initial state x_0 whenever no confusion can arise and simply write $x(t)$.

Symplectic maps enjoy several fundamental properties; see, e.g., [1]. In particular, $\det(D\Psi) = 1$, so that phase-space volume is preserved and clouds of initial conditions are neither spuriously compressed nor dilated. Symplectic maps are locally invertible, and the inverse of a symplectomorphism (a diffeomorphism preserving the symplectic structure) is again symplectic, which permits forward-backward evolution without loss of structure. They are also closed under composition, so any finite sequence of symplectic maps remains symplectic. In practice, the flow map of a Hamiltonian system typically does not admit an explicit closed-form expression and must be approximated by a time discretization method. To preserve the structural properties of the exact symplectic flow in the discrete setting, one commonly employs symplectic integrators [2], which in applications often outperform general-purpose integrators that may lead to spurious energy gain or loss over long time intervals.

One example of such an integrator is the symplectic Euler method,

$$x_{i+1} = x_i + \Delta t J_{2n} \nabla \mathcal{H}(q_i, p_{i+1}), \quad (2)$$

with $x_i = (q_i, p_i)^\top$, where the update map

$$\Psi_{\text{Euler}} : x_i \mapsto x_{i+1}$$

is symplectic for every fixed $\Delta t > 0$ and every $\mathcal{H} \in C^1(\mathbb{R}^{2n}, \mathbb{R})$ (provided the implicit equation (2) admits a solution), see [2, Theorem 3.3]. Furthermore, although symplectic integrators are typically implicit for general Hamiltonians, the symplectic Euler scheme becomes explicit when the Hamiltonian is separable, i.e., $\mathcal{H}(q, p) = T(p) + V(q)$.

Moreover, backward-error analysis shows that a symplectic integrator exactly preserves a modified Hamiltonian that is close to the original one; see [2]. This explains the frequently observed bounded, typically oscillatory error in the Hamiltonian,

$$e_{\mathcal{H}}(t) := |\mathcal{H}(x_0) - \mathcal{H}(x_{\text{approx}}(t))|, \quad t \in \mathbb{T}_{\Delta t} := \{k\Delta t | k \in \mathbb{N}_0\}$$

over very long time horizons, where $x_{\text{approx}}(t)$ denotes the approximate solution obtained by numerical time integration.

The overall objective of this work is the simulation of Hamiltonian dynamics over long time horizons. However, symplectic time stepping can be computationally expensive, as stability and accuracy constraints often enforce small time steps. Therefore, we seek an approximation of the flow

map that enables fast predictions for large time steps $\Delta T = K\Delta t \gg \Delta t$. Kernel methods are particularly attractive here because they yield an RKHS-based learning problem with a closed-form solution (via Hermite–Birkhoff (HB) interpolation), provide direct access to derivatives through reproducing identities, and come with rigorous approximation and convergence theory, including greedy sparsification strategies and show good results in practice [3, 4, 5, 6]. In the kernel setting, Hermite–Birkhoff (HB) interpolation, and more generally Hermite-type kernel interpolation, is widely used across diverse applications, including surface reconstruction [7], PDE discretization [8], image reconstruction [9], and optimal control [10]. In contrast, we leverage HB interpolation to construct a prediction map that is symplectic by construction.

In addition, the mapping defined by the kernel model should be symplectic in order to reflect the physical structure of the flow map and preserve its qualitative properties. The central idea of our symplectic predictor is that, for a given $x_0 \in \mathbb{R}^{2n}$, we solve the implicit system

$$x_{\Delta T, \text{pred}} = x_0 + \Delta T J_{2n} \nabla s(q_0, p_{\Delta T, \text{pred}}), \quad (3)$$

and obtain a prediction $x_{\Delta T, \text{pred}} = (q_{\Delta T, \text{pred}}, p_{\Delta T, \text{pred}})$, where $s : \mathbb{R}^{2n} \rightarrow \mathbb{R}$ is a learned, differentiable, scalar-valued surrogate kernel model. The resulting update map

$$\Psi_s : x_0 \mapsto x_{\Delta T, \text{pred}}$$

is symplectic, since it reflects the symplectic Euler scheme applied to a Hamiltonian system with Hamiltonian s and time step size ΔT .

To train our kernel model, we fix initial states

$$x_0^j = (q_0^j, p_0^j)^\top \in \mathbb{R}^{2n}, \quad j = 1, \dots, M,$$

and compute the corresponding time- ΔT propagated states (i.e., approximated solution after one macro time step, i.e., at ΔT using a symplectic integrator with small time step size Δt)

$$x_{\Delta T}^j = (q_{\Delta T}^j, p_{\Delta T}^j)^\top = \Phi^{\Delta T} (x_0^j) \quad j = 1, \dots, M.$$

Based on these data, we define the input–target pairs

$$\xi_j := (q_0^j, p_{\Delta T}^j)^\top, \quad y_j := J_{2n}^\top \frac{x_{\Delta T}^j - x_0^j}{\Delta T}, \quad j = 1, \dots, M.$$

The mixed argument $\xi_j = (q_0^j, p_{\Delta T}^j)^\top$ reflects the symplectic Euler mixed argument (q_i, p_{i+1}) in (3); with this choice, the identity

$$\nabla s(\xi_j) = J_{2n}^\top \frac{x_{\Delta T}^j - x_0^j}{\Delta T} = y_j \quad j = 1, \dots, M$$

follows directly from (3). Interpreting y_j as a (discrete-time) approximation of the gradient of a scalar potential $u : \mathbb{R}^{2n} \rightarrow \mathbb{R}$ evaluated at ξ_j , the learning task can be recast as a Hermite–Birkhoff (HB) interpolation problem:

$$\nabla s(\xi_j) = y_j, \quad j = 1, \dots, M. \quad (4)$$

Since the symplectic Euler rule only involves the gradient of the function \mathcal{H} , we only aim at good gradient approximation, while the absolute values of s are of secondary importance, i.e., we do not aim to approximate the target Hamiltonian itself. For background on HB interpolation for kernel-based models, we refer to [11, Chapter 16.2].

Similar ideas have recently been studied, mainly in the context of neural networks. Early work on structure-aware learning for Hamiltonian dynamics focused on identifying the energy function

itself. Hamiltonian Neural Networks (HNNs) [12] learn a scalar Hamiltonian \mathcal{H}_{NN} from data and recover the dynamics via

$$\dot{x} = J_{2n} \nabla \mathcal{H}_{\text{NN}}(x), \quad (5)$$

thereby encoding conservation of \mathcal{H}_{NN} along the trajectories. In [13], the training procedure of HNNs is analyzed and a symplectic training scheme is proposed that enforces discrete symplecticity via a symplectic–integrator–based loss, yielding improved long-horizon stability and accuracy compared to standard HNN training. A related approach for approximating time-series data by a learned Hamiltonian system is presented in [14], where a Gaussian process is employed for learning the real Hamiltonian and the dynamics are recovered similarly to (5). Building on the idea of learning a Hamiltonian from data and coupling it with symplectic time integration, [15] restricts to separable Hamiltonians, $\mathcal{H}(q, p) = T(p) + V(q)$, and performs time stepping with a symplectic integrator. This couples a learned, physics-informed model with a geometry-preserving discretization, improving the long-time behavior. In [16], symplectic ODE-Nets are introduced, which enforce Hamiltonian dynamics within the network architecture to learn the underlying dynamics. By explicitly encoding the structure, these models achieve improved generalization with fewer training samples.

A number of approaches learn the flow directly as a symplectic map, without explicitly recovering an underlying Hamiltonian. SympNets [17] compose simple symplectic building blocks (rendering the resulting map symplectic by construction) to approximate the time stepping map. In [18], HénonNets are developed, which concatenate Hénon-like maps and thus offer greater architectural flexibility than SympNets. Furthermore, [19] introduces Generating Function Neural Networks (GFNNs), which learn a generating function whose associated canonical transformation implicitly defines a symplectic map. More recently, [20] unifies and generalizes many of these approaches via Generalized Hamiltonian Neural Networks (GHNNs), which encompass separable-HNN models [15], direct symplectic-map learners [17, 18], and related architectures within a common framework of enhanced expressivity. Several of these recent approaches address long-time step prediction by concatenating multiple learned, separable Hamiltonians and composing their symplectic flows to span a large step [17, 20]. This leverages the fact that a concatenation of symplectic maps remains symplectic. Separable Hamiltonians are popular in these NN architectures because they align with many mechanical systems, yield an explicit and symplectic update (e.g., via symplectic Euler), and thus make training both computationally efficient (since no differentiation through an inner nonlinear solver is required) and structurally well-posed.

In contrast, we learn a single, general (non-separable) Hamiltonian $s(q, p)$ which does not need to approximate the original Hamiltonian and perform prediction over a large horizon ΔT in one implicit symplectic–Euler–type step.

Our key contributions are as follows:

1. We propose a kernel-based scheme for learning and predicting Hamiltonian dynamics that is symplectic by construction and tailored to large time horizons.
2. We provide a detailed analysis of existence and feasibility conditions, i.e., conditions under which a function satisfying the interpolation constraints exists and is uniquely determined. Moreover, we derive convergence results for the symplectic predictor, including a convergence analysis for first-derivative Hermite–Birkhoff interpolation.
3. We combine the kernel model with model order reduction (MOR) [21, 22], rendering the approach computationally feasible also for high-dimensional problems.
4. We present numerical experiments that demonstrate the accuracy, long-time structure preservation, and efficiency of our method.

For our method, one might ask whether an explicit predictor could be obtained by reconstructing a single, separable learned Hamiltonian of the form

$$s(q, p) = s_p(p) + s_q(q).$$

In this case, the corresponding Hermite–Birkhoff interpolation problem would formally read

$$\begin{aligned} \frac{q_{\Delta T}^j - q_0^j}{\Delta T} &= \nabla_p s_p(p_{\Delta T}^j), \\ -\frac{p_{\Delta T}^j - p_0^j}{\Delta T} &= \nabla_q s_q(q_0^j), \end{aligned}$$

with $(q_{\Delta T}^j, p_{\Delta T}^j)^\top = \Phi^{\Delta T} (q_0^j, p_0^j)^\top$. In general, this system is not well-posed: the right-hand side of the second equation can only learn a dependence on q_0^j , whereas the left-hand side typically depends on both q_0^j and p_0^j , i.e., the dependence on p_0^j in the second equation cannot be reflected by this approach (and analogously for the first equation). In Figure 1 we illustrate this issue by plotting the data points

$$\left(p_{\Delta T}^j, \frac{q_{\Delta T}^j - q_0^j}{\Delta T} \right) \quad \text{and} \quad \left(q_0^j, -\frac{p_{\Delta T}^j - p_0^j}{\Delta T} \right),$$

and observe that these data are not well-suited for an interpolation approach based on a separable Hamiltonian since for each input value there are several output values. For comparison, we also present the same type of plot for the data points

$$\left((q_0^j, p_{\Delta T}^j), \frac{q_{\Delta T}^j - q_0^j}{\Delta T} \right) \quad \text{and} \quad \left((q_0^j, p_{\Delta T}^j), -\frac{p_{\Delta T}^j - p_0^j}{\Delta T} \right),$$

and observe that, in this case, there is only one output for each input.

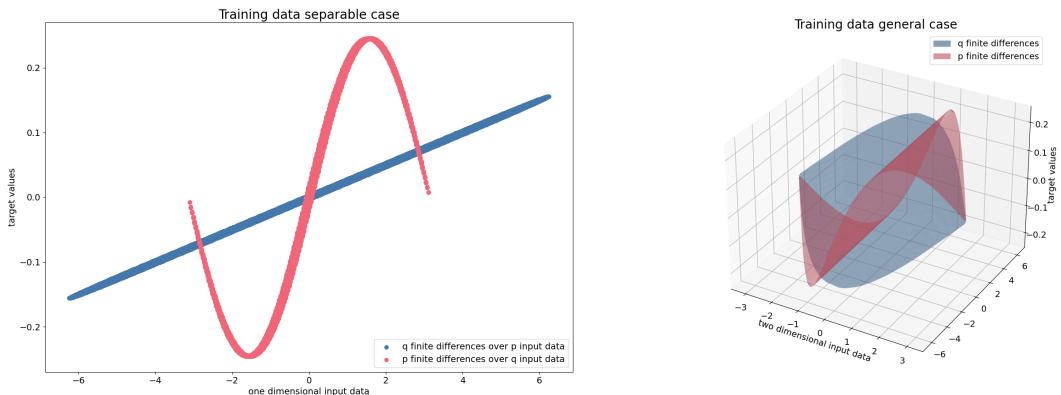


Figure 1: Comparison of the training data for the explicit and implicit method with training data from the whole domain

The remainder of this work is structured as follows. Section 2 reviews kernel-based (generalized) interpolation. Section 3 investigates conditions under which an exact solution exists, which we subsequently approximate by our kernel-based scheme. Section 4 reports numerical results, and Section 5 concludes and outlines directions for future work.

2 Background on Generalized Kernel Interpolation

Let Ω be a nonempty set. A kernel is a symmetric function $k : \Omega \times \Omega \rightarrow \mathbb{R}$. For a finite set of points $X_M := \{x_1, \dots, x_M\} \subset \Omega$, the matrix

$$K_{X_M} := (k(x_i, x_j))_{i,j=1}^M \in \mathbb{R}^{M \times M}$$

is called the Gramian matrix of k (with respect to X_M).

We call k positive definite (p.d.) if, for all $M \in \mathbb{N}$, all finite sets $X_M \subset \Omega$, the Gramian matrix K_{X_M} is symmetric positive semidefinite. We call k strictly positive definite (s.p.d.) if, for all $M \in \mathbb{N}$ and all sets $X_M \subset \Omega$ consisting of pairwise distinct points, the matrix K_{X_M} is symmetric positive definite.

A reproducing kernel Hilbert space (RKHS) $H_k(\Omega)$ over Ω is a Hilbert space of functions $f : \Omega \rightarrow \mathbb{R}$ in which all point evaluation functionals are continuous. For every RKHS there exists a function k — the reproducing kernel — such that $k(\cdot, x) \in H_k(\Omega)$ and the reproducing property

$$f(x) = \langle f, k(\cdot, x) \rangle_{H_k(\Omega)} \quad \text{for all } f \in H_k(\Omega), x \in \Omega,$$

holds.

Moreover, the reproducing property extends to derivatives. In particular, if $\Omega \subset \mathbb{R}^{2n}$ and $k \in C^2(\Omega \times \Omega)$, then (for suitable $H_k(\Omega)$) the first-order partial derivative point evaluation functionals are continuous, and

$$\partial_\ell f(x) = \langle f, \partial_\ell^{(2)} k(\cdot, x) \rangle_{H_k(\Omega)} \quad \text{for all } f \in H_k(\Omega), x \in \Omega, \ell = 1, \dots, 2n, \quad (6)$$

where $\partial_\ell^{(2)}$ denotes the ℓ -th partial derivative of k with respect to its second argument.

Conversely, every p.d. kernel k induces a unique RKHS $H_k(\Omega)$, i.e., there is a one-to-one correspondence between p.d. kernels and RKHSs.

In an RKHS $H_k(\Omega)$, we can formulate an abstract generalized interpolation problem of the form

$$s_M = \underset{s \in H_k(\Omega)}{\operatorname{argmin}} \left\{ \|s\|_{H_k(\Omega)} \mid \lambda_j(s) = y_j \text{ for } j = 1, \dots, M \right\}, \quad (7)$$

where $\lambda_1, \dots, \lambda_M \in H_k(\Omega)'$ are linearly independent, continuous linear functionals, and y_1, \dots, y_M are prescribed target values.

By the Riesz representation theorem in an RKHS, for each λ_i there exists a unique $v_i \in H_k(\Omega)$ such that

$$\lambda_i(f) = \langle f, v_i \rangle_{H_k(\Omega)} \quad \text{for all } f \in H_k(\Omega).$$

If $k(\cdot, \cdot)$ is the reproducing kernel of $H_k(\Omega)$, then v_i can be expressed explicitly as

$$v_i(x) = \left(\lambda_i^{(2)} k \right) (x) = \lambda_i(k(x, \cdot)),$$

i.e., λ_i acts on the second argument of k . For a vector of functionals $\Lambda_M = [\lambda_1, \dots, \lambda_M]$, we define the generalized Gramian matrix $G_\Lambda \in \mathbb{R}^{M \times M}$ by

$$(G_\Lambda)_{ij} := \langle v_j, v_i \rangle_{H_k(\Omega)} = \lambda_i^{(1)} \lambda_j^{(2)} k \quad (i, j = 1, \dots, M).$$

By [11, Theorem 16.1], if $\lambda_1, \dots, \lambda_M$ are linearly independent on $H_k(\Omega)$, then for every $y \in \mathbb{R}^M$ there exists a unique minimum-norm interpolant (in the sense of (7)), which has the form

$$s(\cdot) = \sum_{j=1}^M c_j v_j(\cdot) = \sum_{j=1}^M c_j \lambda_j^{(2)} k(\cdot, \cdot), \quad \text{with } G_\Lambda c = y.$$

A special case of the generalized interpolation problem is the Hermite–Birkhoff (HB) interpolation corresponding to (4). For this, let $X_M = \{x_j\}_{j=1}^M \subset \Omega \subset \mathbb{R}^{2n}$ and, for each j , let $\alpha_j \in \{1, \dots, 2n\}$ be a coordinate index. We define linear functionals

$$\lambda_j(f) := \lambda_{j,\alpha_j}(f) := \partial_{\alpha_j} f(x_j), \quad j = 1, \dots, M.$$

These functionals are linearly independent on H_k if, for $i \neq j$, either $\alpha_i \neq \alpha_j$ or $x_i \neq x_j$ and k is a strictly positive definite, translation-invariant kernel of the form $k(x, x') = \phi(x - x')$ with $\phi \in L^1(\mathbb{R}^d) \cap C^2(\mathbb{R}^d)$; see [11, Theorem 16.4].

Moreover, for $k \in C^2(\Omega \times \Omega)$, the functionals are continuous on $H_k(\Omega)$ by the derivative reproducing property (6).

In the HB setting, the Riesz representers and the corresponding generalized Gramian matrix entries are given by

$$v_j(x) = \partial_{\alpha_j}^{(2)} k(x, x_j), \quad G_{i,j} = \partial_{\alpha_i}^{(1)} \partial_{\alpha_j}^{(2)} k(x_i, x_j).$$

Hence, the interpolant takes the form

$$s(x) = \sum_{j=1}^M c_j \partial_{\alpha_j}^{(2)} k(x, x_j), \quad (8)$$

where the coefficients c_j , $j = 1, \dots, M$, are obtained from the linear system

$$G_{\Lambda} c = y,$$

with $c := (c_1, \dots, c_M)^\top$, data vector $y := (y_1, \dots, y_M)^\top$, and G_{Λ} the generalized Gramian matrix. If the family $\{\lambda_j\}_{j=1}^M$ is linearly independent, this system is uniquely solvable, and the interpolant exists uniquely [11, Theorem 16.5].

2.1 Convergence rates for gradient-Hermite-Birkhoff f -greedy

For large M , solving the dense linear system and evaluating (8) become computationally expensive and can suffer from ill-conditioning. A common strategy is therefore to select a much smaller subset $\Lambda_{m_{\max}} \subset \Lambda_M$ with $m_{\max} \ll M$. Greedy algorithms—such as VKOGA [23, 24]—expand the active set Λ_m iteratively according to a selection rule using the current interpolant s_{f,Λ_m} . A popular choice is the f -greedy rule, which starts with $\Lambda_0 = \emptyset$ and $s_{f,\Lambda_0} = 0$ and at iteration $m \geq 0$ selects

$$\lambda_{m+1} \in \operatorname{argmax}_{\lambda_j \in \Lambda_M} |y_j - \lambda_j(s_{f,\Lambda_m})|, \quad \Lambda_{m+1} := \Lambda_m \cup \{\lambda_{m+1}\}, \quad (9)$$

where the residuals at already selected functionals vanish, i.e., $y_j - \lambda_j(s_{f,\Lambda_m}) = 0$, $j = 1, \dots, m$. Other sparsification strategies tailored to function interpolation (and not HB interpolation) include ℓ_1 -penalization [25] and support vector regression (SVR) [4].

In the context of Hermite–Birkhoff interpolation, we now formalize the f -greedy strategy more precisely.

For a finite selection

$$\{(x_i, \ell_i)\}_{i=1}^m \subset \Omega \times \mathcal{J},$$

with index set $\mathcal{J} := \{1, \dots, n\}$ (where n is the ambient dimension of Ω), define

$$V_m := \operatorname{span} \left\{ \partial_{\ell_i}^{(2)} k(\cdot, x_i) : i = 1, \dots, m \right\}, \quad \Pi_m : H_k(\Omega) \rightarrow V_m$$

to be the orthogonal projector onto V_m . Given a target function $u \in H_k(\Omega)$, we set $s_m := \Pi_m u$ and $e_m := u - s_m$.

Then the f -greedy selection can be formulated as follows: for $m \geq 0$, choose

$$(x_{m+1}, \ell_{m+1}) \in \operatorname{argmax}_{x \in \Omega, \ell \in \mathcal{J}} |\partial_\ell e_m(x)|,$$

and set $s_{m+1} := \Pi_{m+1} u$.

Greedy schemes produce sparse surrogates and come with rigorous—sometimes even optimal—convergence guarantees [26, 27, 28]. For HB interpolation, greedy convergence has been investigated in [10] and, in more general functional settings, in [29, 30]. The application-oriented work [10] establishes convergence of a target-dependent greedy Hermite kernel scheme (based on an f -type selection rule) for value-function surrogates in optimal control. In contrast, [29] studies well-posed operator equations in an abstract Hilbert-space framework and relates greedy convergence rates to Kolmogorov n -widths of the underlying representer set, without specializing to the Hermite case. Complementarily, [30] develops a convergence theory for generalized kernel-based interpolation with totally bounded sets of sampling functionals, which in particular covers HB interpolation. In the following, we extend the f -greedy convergence rates from [26, 31] to our gradient–HB case. We begin with the following theorem, which provides a bound on the maximum derivative error.

Theorem 1 (First-order HB bound). *Let $u \in H_k(\Omega)$, $\Omega \subset \mathbb{R}^n$, and apply the f -greedy algorithm of the previous subsection with index set $\mathcal{J} := \{1, \dots, 2n\}$. Then, for every $m \geq 1$,*

$$\min_{m+1 \leq i \leq 2m} \|\nabla e_i\|_{L^\infty(\Omega)} \leq \sqrt{nm}^{-1/2} \|e_{m+1}\|_{H_k(\Omega)} \left[\prod_{i=m+1}^{2m} P_i(x_{i+1}, \ell_{i+1}) \right]^{1/m}, \quad (10)$$

where the (derivative) power function is defined by

$$P_m(x, \ell) := \|(I - \Pi_m) \partial_\ell^{(2)} k(\cdot, x)\|_{H_k(\Omega)}, \quad (x, \ell) \in \Omega \times \mathcal{J}.$$

Proof. The proof proceeds similarly to the β -greedy analysis in [26, 31] (with $\beta = 1$). \square

For completeness it is given in the appendix under Proof of Theorem 1.

In the remainder of this section, we study the convergence of the symplectic predictor. To this end, we introduce a type II generating function, i.e., a generating function expressed in the mixed variables $(q_0, p_{\Delta T})$. For background on the different generating-function types, see [32].

Definition 1 (Type II generating function). *Let $\Phi^{\Delta T} : D \rightarrow \mathbb{R}^{2n}$ and define*

$$\Omega := \{I_1 x_0 + I_2 \Phi^{\Delta T}(x_0) : x_0 \in D\}, \quad I_1 := \begin{bmatrix} I_n & 0 \\ 0 & 0 \end{bmatrix}, \quad I_2 := \begin{bmatrix} 0 & 0 \\ 0 & I_n \end{bmatrix}.$$

A function $S^{\Delta T} \in H_k(\Omega) \cap C^1(\Omega)$ is called a type II generating function (for $\Phi^{\Delta T}$ on Ω) if, for all $x_0 \in D$,

$$J_{2n}^\top \frac{\Phi^{\Delta T}(x_0) - x_0}{\Delta T} = \nabla S^{\Delta T}(I_1 x_0 + I_2 \Phi^{\Delta T}(x_0)). \quad (11)$$

With Definition 1 in place, we establish how the convergence rate for the gradient approximation in Theorem 1 propagates to a corresponding convergence rate for the symplectic predictor.

Theorem 2 (Convergence rate for the prediction error). *Let $S^{\Delta T} \in C^2(\Omega)$ be a type-II generating function of the time- ΔT Hamiltonian flow $\Phi^{\Delta T}$, defined on an open, convex set $\Omega \subset \mathbb{R}^{2n}$ of mixed variables $(q_0, p_{\Delta T})$. Assume $S^{\Delta T} \in H_k(\Omega)$ and that $s_{i_m} \in H_k(\Omega)$ is obtained by the HB f -greedy procedure from the previous subsection, where we choose an index $i_m \in \{m+1, \dots, 2m\}$ such that*

$$\|\nabla e_{i_m}\|_{L^\infty(\Omega)} = \min_{m+1 \leq i \leq 2m} \|\nabla e_i\|_{L^\infty(\Omega)}.$$

Fix a compact set $K \subset \mathbb{R}^{2n}$ and assume:

(i) **Uniform solvability.** For every $x_0 \in K$ and every m sufficiently large, the implicit equations

$$y = x_0 + \Delta T J_{2n} \nabla S^{\Delta T} (I_1 x_0 + I_2 y), \quad y = x_0 + \Delta T J_{2n} \nabla s_{i_m} (I_1 x_0 + I_2 y),$$

admit unique solutions $y^* = \Phi^{\Delta T}(x_0)$ and $y_m = x_{\Delta T, i_m}(x_0)$, respectively, and satisfy

$$I_1 x_0 + I_2 y^* \in \Omega, \quad I_1 x_0 + I_2 y_m \in \Omega.$$

(ii) **Uniform Lipschitz continuity in y .** There exists $L_S > 0$ such that

$$\sup_{\substack{x_0 \in K \\ y: I_1 x_0 + I_2 y \in \Omega}} \|\nabla^2 S^{\Delta T} (I_1 x_0 + I_2 y) I_2\|_2 = L_S < \infty.$$

Assume that

$$\Delta T < \frac{1}{L_S}. \quad (12)$$

Then there exists a constant $C > 0$, independent of m and x_0 , such that

$$\sup_{x_0 \in K} \|x_{\Delta T, i_m}(x_0) - \Phi^{\Delta T}(x_0)\|_2 \leq C \Delta T \sqrt{2n} m^{-1/2} \|e_{m+1}\|_{H_k(\Omega)} \left[\prod_{i=m+1}^{2m} P_i(x_{i+1}, \ell_{i+1}) \right]^{1/m}.$$

Proof. Fix $x_0 \in K$ and denote by $y^* = \Phi^{\Delta T}(x_0)$ and $y_m = x_{\Delta T, i_m}(x_0)$ the exact and approximate predictors, respectively. Define

$$F_m(y; x_0) := y - x_0 - \Delta T J_{2n} \nabla s_{i_m} (I_1 x_0 + I_2 y), \quad F(y; x_0) := y - x_0 - \Delta T J_{2n} \nabla S^{\Delta T} (I_1 x_0 + I_2 y).$$

By construction,

$$0 = F_m(y_m; x_0) = y_m - x_0 - \Delta T J_{2n} \nabla s_{i_m} (I_1 x_0 + I_2 y_m).$$

Subtracting from $F(y_m; x_0)$ yields

$$F(y_m; x_0) = -\Delta T J_{2n} (\nabla S^{\Delta T} - \nabla s_{i_m}) (I_1 x_0 + I_2 y_m) = -\Delta T J_{2n} \nabla e_{i_m} (I_1 x_0 + I_2 y_m).$$

Hence, using $\|J_{2n}\|_2 = 1$,

$$\|F(y_m; x_0)\|_2 \leq \Delta T \|\nabla e_{i_m}\|_{L^\infty(\Omega)}. \quad (13)$$

Since $F(y^*; x_0) = 0$, the integral form of the multivariate mean value theorem gives

$$F(y_m; x_0) = \int_0^1 D_y F(y^* + \theta(y_m - y^*); x_0) d\theta (y_m - y^*).$$

with

$$D_y F(y; x_0) := I_{2n} - \Delta T J_{2n} \nabla^2 S^{\Delta T} (I_1 x_0 + I_2 y) I_2.$$

Define

$$A_m(x_0) := \int_0^1 D_y F(y^* + \theta(y_m - y^*); x_0) d\theta.$$

Set

$$B(y; x_0) := \Delta T J_{2n} \nabla^2 S^{\Delta T} (I_1 x_0 + I_2 y) I_2, \text{ such that } D_y F(y; x_0) = I_{2n} - B(y; x_0).$$

Define the averaged operator

$$\bar{B}_m(x_0) := \int_0^1 B(y^* + \theta(y_m - y^*); x_0) d\theta, \text{ such that } A_m(x_0) = I_{2n} - \bar{B}_m(x_0).$$

Since Ω is convex and $I_1x_0 + I_2y^*, I_1x_0 + I_2y_m \in \Omega$, the entire segment lies in Ω . By assumption (ii),

$$\|\bar{B}_m(x_0)\|_2 \leq \Delta T L_S < 1.$$

Therefore $A_m(x_0)$ is invertible and admits the Neumann series

$$A_m(x_0)^{-1} = \sum_{k=0}^{\infty} \bar{B}_m(x_0)^k,$$

and further

$$\|A_m(x_0)^{-1}\|_2 \leq \frac{1}{1 - \Delta T L_S} =: C_{\text{inv}}.$$

Consequently,

$$y_m - y^* = A_m(x_0)^{-1} F(y_m; x_0),$$

and

$$\|y_m - y^*\|_2 \leq C_{\text{inv}} \|F(y_m; x_0)\|_2.$$

Combining with the bound (13) and Theorem 1 yields

$$\sup_{x_0 \in K} \|x_{\Delta T, i_m}(x_0) - \Phi^{\Delta T}(x_0)\|_2 \leq C \Delta T \sqrt{2n} m^{-1/2} \|e_{m+1}\|_{H_k(\Omega)} \left[\prod_{i=m+1}^{2m} P_i(x_{i+1}, \ell_{i+1}) \right]^{1/m},$$

with $C := C_{\text{inv}}$. □

In summary, the gradient–HB f -greedy strategy yields a quantitative decay bound for the maximal derivative error (Theorem 1), and Theorem 2 shows that this decay translates to a uniform convergence rate for the symplectic predictor on compact subsets.

3 On the Existence of the Target Function

To obtain provable convergence guarantees, we assume that the generating function belongs to the RKHS $H_k(\Omega)$. In our setting, however, it is not a priori clear under which conditions there even exists a differentiable function $S^{\Delta T}$ that satisfies the interpolation constraint

$$J_{2n}^\top \frac{\Phi^{\Delta T}(x_0) - x_0}{\Delta T} = \nabla S^{\Delta T}(I_1x_0 + I_2\Phi^{\Delta T}(x_0)). \quad (14)$$

When such a function $S^{\Delta T}$ exists and, in addition, $S^{\Delta T} \in H_k(\Omega)$ on the mixed-data domain

$$\Omega := \{I_1x_0 + I_2\Phi^{\Delta T}(x_0) : x_0 \in D \subset \mathbb{R}^{2n}\},$$

the HB interpolation convergence analysis from the previous section applies. Existence of such an $S^{\Delta T}$ is not automatic: the discrete flow increment must be representable as the gradient of a scalar function of the mixed variables $(q_0, p_{\Delta T})$. We make this precise and provide verifiable conditions in this section. First, we provide a general statement with abstract conditions on the flow map $\Phi^{\Delta T}$ under which a generating function exists. Since the proof of the following theorem involves locally inverting the flow map, the variables q, p become functions of the output variables. To indicate whether a symbol is treated as a function or as a variable, we display functions in bold throughout this section.

Theorem 3 (Existence of a generating function). *Let $\mathcal{H} \in C^2(\Omega)$, $\Omega \subset \mathbb{R}^{2n}$, and let $\Phi^{\Delta T} : \Omega \rightarrow \Phi^{\Delta T}(\Omega)$ be the flow map for a fixed $\Delta T > 0$. Write ¹*

$$\Phi^{\Delta T}(q, p) = (\mathbf{Q}(q, p), \mathbf{P}(q, p)),$$

and denote the Jacobian of $\Phi^{\Delta T}$ with respect to (q, p) by

$$D\Phi^{\Delta T}(q, p) = \begin{pmatrix} \frac{\partial}{\partial q} \mathbf{Q} & \frac{\partial}{\partial p} \mathbf{Q} \\ \frac{\partial}{\partial q} \mathbf{P} & \frac{\partial}{\partial p} \mathbf{P} \end{pmatrix} =: \begin{pmatrix} \mathbf{A}(q, p) & \mathbf{B}(q, p) \\ \mathbf{C}(q, p) & \mathbf{D}(q, p) \end{pmatrix},$$

where $\mathbf{A}, \mathbf{B}, \mathbf{C}, \mathbf{D} : \Omega \rightarrow \mathbb{R}^{n \times n}$.

Fix an open set $U \subset \Omega$ such that:

(i) $\mathbf{D}(q, p)$ is invertible for all $(q, p) \in U$;

(ii) The map

$$\Psi : U \rightarrow W, \quad \Psi(q, p) := (q, \mathbf{P}(q, p)),$$

is a diffeomorphism onto a simply connected open set $W \subset \mathbb{R}^{2n}$.

Then there exist functions $\mathbf{p}, \mathbf{Q} \in C^1(W, \mathbb{R}^n)$, unique up to an additive constant in S , such that, if we view them as functions of $(q, P) \in W$ via

$$(q, P) = \Psi(q, p), \quad (Q, P) = \Phi^{\Delta T}(q, p),$$

i.e. $(q, p) = \Psi^{-1}(q, P)$ and $(Q, P) = \Phi^{\Delta T}(q, \mathbf{p}(q, P)) = (\mathbf{Q}(q, P), P)$, then

$$\mathbf{p}(q, P) = \partial_q S(q, P), \quad \mathbf{Q}(q, P) = \partial_P S(q, P).$$

Moreover, the type-II generating function

$$S^{\Delta T}(q, P) := \frac{1}{\Delta T} (S(q, P) - q^\top P)$$

satisfies, for all $x = (q, p) \in U$,

$$J_{2n}^\top \frac{\Phi^{\Delta T}(x) - x}{\Delta T} = \nabla_{(q, P)} S^{\Delta T} (I_1 x + I_2 \Phi^{\Delta T}(x)).$$

Proof. Recall $\Psi(q, p) := (q, \mathbf{P}(q, p))$ and

$$D\Psi(q, p) = \begin{pmatrix} \frac{\partial}{\partial q} q & \frac{\partial}{\partial p} q \\ \frac{\partial}{\partial q} \mathbf{P} & \frac{\partial}{\partial p} \mathbf{P} \end{pmatrix} = \begin{pmatrix} I_n & 0 \\ \mathbf{C}(q, p) & \mathbf{D}(q, p) \end{pmatrix}.$$

By assumption (i), $\mathbf{D}(q, p)$ is invertible on U , so $D\Psi(q, p)$ is invertible and, by the Implicit Function Theorem, Ψ is locally invertible on U . Hence there exists a C^1 function $\mathbf{p} = \mathbf{p}(q, P)$ on W such that

$$\mathbf{P}(q, \mathbf{p}(q, P)) = P.$$

We then define

$$\mathbf{Q}(q, P) := \mathbf{Q}(q, \mathbf{p}(q, P)).$$

Since $\Phi^{\Delta T}$ is symplectic, we have

$$(D\Phi^{\Delta T}(q, p))^\top J_{2n} D\Phi^{\Delta T}(q, p) = J_{2n}.$$

¹Note that, for brevity, we suppress the explicit dependence on ΔT in \mathbf{Q}, \mathbf{P} and their derivatives whenever no confusion can arise.

Writing

$$D\Phi^{\Delta T}(q, p) = \begin{pmatrix} \mathbf{A} & \mathbf{B} \\ \mathbf{C} & \mathbf{D} \end{pmatrix},$$

and using the symplecticity condition this implies

$$\begin{pmatrix} 0 & I_n \\ -I_n & 0 \end{pmatrix} = J_{2n} = (D\Phi^{\Delta T})^\top J_{2n} D\Phi^{\Delta T} = \begin{pmatrix} \mathbf{A}^\top & \mathbf{C}^\top \\ \mathbf{B}^\top & \mathbf{D}^\top \end{pmatrix} \begin{pmatrix} 0 & I_n \\ -I_n & 0 \end{pmatrix} \begin{pmatrix} \mathbf{A} & \mathbf{B} \\ \mathbf{C} & \mathbf{D} \end{pmatrix} \\ = \begin{pmatrix} \mathbf{A}^\top \mathbf{C} - \mathbf{C}^\top \mathbf{A} & \mathbf{A}^\top \mathbf{D} - \mathbf{C}^\top \mathbf{B} \\ \mathbf{B}^\top \mathbf{C} - \mathbf{D}^\top \mathbf{A} & \mathbf{B}^\top \mathbf{D} - \mathbf{D}^\top \mathbf{B} \end{pmatrix},$$

holding pointwise.

With \mathbf{D} invertible, these identities imply

$$\mathbf{B}\mathbf{D}^{-1} = (\mathbf{B}\mathbf{D}^{-1})^\top, \quad \mathbf{A} - \mathbf{B}\mathbf{D}^{-1}\mathbf{C} = \mathbf{D}^{-\top}, \quad \mathbf{D}^{-1}\mathbf{C} = (\mathbf{D}^{-1}\mathbf{C})^\top. \quad (15)$$

Indeed:

1. From $\mathbf{B}^\top \mathbf{D} = \mathbf{D}^\top \mathbf{B}$, multiplying on the right by \mathbf{D}^{-1} and on the left by $\mathbf{D}^{-\top}$ gives

$$\mathbf{D}^{-\top} \mathbf{B}^\top = \mathbf{B}\mathbf{D}^{-1},$$

i.e., $\mathbf{B}\mathbf{D}^{-1}$ is symmetric.

2. From $\mathbf{B}^\top \mathbf{C} - \mathbf{D}^\top \mathbf{A} = -I_n$, multiplying on the left by $\mathbf{D}^{-\top}$ yields

$$\mathbf{D}^{-\top} \mathbf{B}^\top \mathbf{C} - \mathbf{A} = -\mathbf{D}^{-\top}.$$

Using $\mathbf{D}^{-\top} \mathbf{B}^\top = (\mathbf{B}\mathbf{D}^{-1})^\top = \mathbf{B}\mathbf{D}^{-1}$ (by symmetry of $\mathbf{B}\mathbf{D}^{-1}$), we obtain

$$\mathbf{A} = \mathbf{B}\mathbf{D}^{-1}\mathbf{C} + \mathbf{D}^{-\top} \implies \mathbf{A} - \mathbf{B}\mathbf{D}^{-1}\mathbf{C} = \mathbf{D}^{-\top}.$$

3. Finally, starting from $\mathbf{A}^\top \mathbf{C} = \mathbf{C}^\top \mathbf{A}$ and inserting $\mathbf{A} = \mathbf{D}^{-\top} + \mathbf{B}\mathbf{D}^{-1}\mathbf{C}$ gives

$$\begin{aligned} \mathbf{A}^\top \mathbf{C} &= (\mathbf{D}^{-\top} + \mathbf{B}\mathbf{D}^{-1}\mathbf{C})^\top \mathbf{C} = \mathbf{D}^{-1}\mathbf{C} + \mathbf{C}^\top \mathbf{D}^{-\top} \mathbf{B}^\top \mathbf{C}, \\ \mathbf{C}^\top \mathbf{A} &= \mathbf{C}^\top (\mathbf{D}^{-\top} + \mathbf{B}\mathbf{D}^{-1}\mathbf{C}) = \mathbf{C}^\top \mathbf{D}^{-\top} + \mathbf{C}^\top \mathbf{B}\mathbf{D}^{-1}\mathbf{C}. \end{aligned}$$

Since $\mathbf{D}^{-\top} \mathbf{B}^\top = \mathbf{B}\mathbf{D}^{-1}$, the second terms agree, and we conclude

$$\mathbf{D}^{-1}\mathbf{C} = \mathbf{C}^\top \mathbf{D}^{-\top} \iff (\mathbf{D}^{-1}\mathbf{C})^\top = \mathbf{D}^{-1}\mathbf{C}.$$

By the local invertibility of Ψ , there is a local solution $\mathbf{p} = \mathbf{p}(q, P)$ of $\mathbf{P}(q, p) = P$, i.e.,

$$\mathbf{P}(q, \mathbf{p}(q, P)) = P.$$

We recall the definition

$$\mathbf{Q}(q, P) = \mathbf{Q}(q, \mathbf{p}(q, P)),$$

and differentiate the identities

$$\mathbf{P}(q, \mathbf{p}(q, P)) = P, \quad \mathbf{Q}(q, \mathbf{p}(q, P)) = Q$$

with respect to q and P .

From $\mathbf{P}(q, \mathbf{p}(q, P)) = P$ we obtain

$$\begin{aligned} \partial_q \mathbf{P} + \partial_p \mathbf{P} \partial_q \mathbf{p} = 0 &\implies \mathbf{C} + \mathbf{D} \frac{\partial \mathbf{p}}{\partial q} = 0 \implies \frac{\partial \mathbf{p}}{\partial q} = -\mathbf{D}^{-1}\mathbf{C}, \\ \partial_p \mathbf{P} \partial_P \mathbf{p} = I_n &\implies \mathbf{D} \frac{\partial \mathbf{p}}{\partial P} = I_n \implies \frac{\partial \mathbf{p}}{\partial P} = \mathbf{D}^{-1}. \end{aligned}$$

From $\mathbf{Q}(q, \mathbf{p}(q, P)) = Q$ we get

$$\begin{aligned}\partial_q \mathbf{Q} + \partial_p \mathbf{Q} \partial_q \mathbf{p} &= \mathbf{A} + \mathbf{B} (-\mathbf{D}^{-1} \mathbf{C}) = \mathbf{A} - \mathbf{B} \mathbf{D}^{-1} \mathbf{C} = \frac{\partial \mathbf{Q}}{\partial q}, \\ \partial_p \mathbf{Q} \partial_P \mathbf{p} &= \mathbf{B} \mathbf{D}^{-1} = \frac{\partial \mathbf{Q}}{\partial P}.\end{aligned}$$

Collecting these four blocks yields

$$\frac{\partial(\mathbf{p}, \mathbf{Q})}{\partial(q, P)} = \begin{pmatrix} -\mathbf{D}^{-1} \mathbf{C} & \mathbf{D}^{-1} \\ \mathbf{A} - \mathbf{B} \mathbf{D}^{-1} \mathbf{C} & \mathbf{B} \mathbf{D}^{-1} \end{pmatrix}.$$

Using the identities in (15), this Jacobian satisfies

$$\frac{\partial \mathbf{p}}{\partial q} = \left(\frac{\partial \mathbf{p}}{\partial q} \right)^\top, \quad \frac{\partial \mathbf{Q}}{\partial P} = \left(\frac{\partial \mathbf{Q}}{\partial P} \right)^\top, \quad \frac{\partial \mathbf{p}}{\partial P} = \left(\frac{\partial \mathbf{Q}}{\partial q} \right)^\top \quad (\text{since } (\mathbf{A} - \mathbf{B} \mathbf{D}^{-1} \mathbf{C})^\top = \mathbf{D}^{-1}).$$

These are precisely the symmetry conditions that are necessary for the existence of a scalar potential S with $\mathbf{p} = \partial_q S$ and $\mathbf{Q} = \partial_P S$.

We now construct such a potential. Fix a reference point $(q_0, P_0) \in W$ and define

$$S(q, P) := \mathcal{I}_1(q) + \mathcal{I}_2(q, P),$$

with

$$\mathcal{I}_1(q) := \int_0^1 \mathbf{p}(q_0 + \tau(q - q_0), P_0)^\top (q - q_0) d\tau, \quad \mathcal{I}_2(q, P) := \int_0^1 \mathbf{Q}(q, P_0 + \tau(P - P_0))^\top (P - P_0) d\tau.$$

Clearly $S(q_0, P_0) = 0$.

For \mathcal{I}_1 , define

$$g(\tau) := \tau \mathbf{p}(q_0 + \tau(q - q_0), P_0).$$

Then

$$g'(\tau) = \mathbf{p}(q_0 + \tau(q - q_0), P_0) + \tau(\partial_q \mathbf{p})(q_0 + \tau(q - q_0), P_0)^\top (q - q_0),$$

and thus

$$\begin{aligned}\partial_q \mathcal{I}_1(q) &= \int_0^1 \left[\mathbf{p}(q_0 + \tau(q - q_0), P_0) + \tau(\partial_q \mathbf{p})(q_0 + \tau(q - q_0), P_0)^\top (q - q_0) \right] d\tau \\ &= \int_0^1 g'(\tau) d\tau = g(1) - g(0) = \mathbf{p}(q, P_0).\end{aligned}$$

For \mathcal{I}_2 , we note that

$$\begin{aligned}\partial_q \left(\mathbf{Q}(q, P_0 + \tau(P - P_0))^\top (P - P_0) \right) &= [(\partial_q \mathbf{Q})(q, P_0 + \tau(P - P_0))]^\top (P - P_0) \\ &= (\partial_P \mathbf{p})(q, P_0 + \tau(P - P_0)) (P - P_0),\end{aligned}$$

where we used the relation $(\partial_q \mathbf{Q})^\top = \partial_P \mathbf{p}$. Furthermore,

$$\frac{d}{d\tau} \mathbf{p}(q, P_0 + \tau(P - P_0)) = (\partial_P \mathbf{p})(q, P_0 + \tau(P - P_0)) (P - P_0),$$

so

$$\begin{aligned}\partial_q \mathcal{I}_2(q, P) &= \int_0^1 (\partial_P \mathbf{p})(q, P_0 + \tau(P - P_0)) (P - P_0) d\tau \\ &= \int_0^1 \frac{d}{d\tau} \mathbf{p}(q, P_0 + \tau(P - P_0)) d\tau \\ &= \mathbf{p}(q, P) - \mathbf{p}(q, P_0).\end{aligned}$$

Combining the two terms, we obtain

$$\partial_q S(q, P) = \partial_q \mathcal{I}_1(q) + \partial_q \mathcal{I}_2(q, P) = \mathbf{p}(q, P_0) + (\mathbf{p}(q, P) - \mathbf{p}(q, P_0)) = \mathbf{p}(q, P).$$

Since \mathcal{I}_1 does not depend on P , we have $\partial_P \mathcal{I}_1 = 0$. For \mathcal{I}_2 , define

$$h(\tau) := \tau \mathbf{Q}(q, P_0 + \tau(P - P_0)).$$

Then

$$h'(\tau) = \mathbf{Q}(q, P_0 + \tau(P - P_0)) + \tau(\partial_P \mathbf{Q})(q, P_0 + \tau(P - P_0))(P - P_0),$$

and hence

$$\begin{aligned} \partial_P \mathcal{I}_2(q, P) &= \int_0^1 [(\partial_P \mathbf{Q})(q, P_0 + \tau(P - P_0)) \tau(P - P_0) + \mathbf{Q}(q, P_0 + \tau(P - P_0))] d\tau \\ &= \int_0^1 h'(\tau) d\tau = h(1) - h(0) = \mathbf{Q}(q, P). \end{aligned}$$

Thus

$$\partial_P S(q, P) = \partial_P \mathcal{I}_1(q) + \partial_P \mathcal{I}_2(q, P) = \mathbf{Q}(q, P).$$

Consequently,

$$\partial_q S(q, P) = \mathbf{p}(q, P), \quad \partial_P S(q, P) = \mathbf{Q}(q, P).$$

Finally, define

$$S^{\Delta T}(q, P) := \frac{1}{\Delta T} (S(q, P) - q^\top P),$$

which yields

$$\nabla_q S^{\Delta T}(q, P) = \frac{\mathbf{p}(q, P) - P}{\Delta T}, \quad \nabla_P S^{\Delta T}(q, P) = \frac{\mathbf{Q}(q, P) - q}{\Delta T}.$$

Evaluating at

$$(q, P) = I_1 x + I_2 \Phi^{\Delta T}(x), \quad x = (q, p),$$

we obtain

$$\nabla_{(q, P)} S^{\Delta T} (I_1 x + I_2 \Phi^{\Delta T}(x)) = \begin{pmatrix} -(P - p)/\Delta T \\ (Q - q)/\Delta T \end{pmatrix} = J_{2n}^\top \frac{\Phi^{\Delta T}(x) - x}{\Delta T},$$

which is the desired identity. \square

Building on the preceding result, we show that the time- ΔT flow map of a Hamiltonian system admits a generating function on any forward-invariant set, provided that ΔT satisfies an explicit step-size restriction. In particular, for C^2 Hamiltonians, choosing ΔT sufficiently small guarantees the existence of a generating function on the considered domain.

Theorem 4 (Uniform invertibility on compact forward-invariant sets). *Let $\mathcal{H} \in C^2(\mathbb{R}^{2n})$ and consider the Hamiltonian system*

$$\dot{x} = J_{2n} \nabla \mathcal{H}(x),$$

with flow Φ^t . Let $K \subset \mathbb{R}^{2n}$ be nonempty, compact, and forward invariant for times in an interval $[0, T]$ (with $T \in (0, \infty]$), i.e. $\Phi^t(K) \subset K$ for all $t \in [0, T]$. Define

$$L_K := \sup_{y \in K} \|\nabla^2 \mathcal{H}(y)\|_2 < \infty.$$

Then, for every $x \in K$ and every fixed ΔT satisfying²

$$0 \leq \Delta T < \Delta T_K^* := \min \left\{ T, \frac{\log 2}{L_K} \right\},$$

²interpret $\frac{\log 2}{L_K} = +\infty$ if $L_K = 0$

on any (q, P) -chart (U, ψ) with $U \cap K \neq \emptyset$ such that the coordinate image $\psi(U) \subset \mathbb{R}^{2n}$ is simply connected, the assumptions of Theorem 3 are satisfied, and there exists a generating function $S(q, P)$ such that, viewing p and Q as functions of (q, P) ,

$$\mathbf{p}(q, P) = \partial_q S(q, P), \quad \mathbf{Q}(q, P) = \partial_P S(q, P),$$

and the generating-function identity from Theorem 3 holds uniformly for all $x \in K$ and all $0 \leq \Delta T < \Delta T_K^*$.

Proof. Fix $x \in K$ and $\Delta T \in [0, T)$. By forward invariance, the trajectory segment $\{\Phi^t(x) : t \in [0, \Delta T]\}$ lies in K . Let

$$\mathbf{Y}(t; x) := D\Phi^t(x).$$

Then \mathbf{Y} solves the differential equation

$$\dot{\mathbf{Y}}(t; x) = DF(\Phi^t(x))\mathbf{Y}(t; x), \quad \mathbf{Y}(0; x) = I_{2n},$$

with $F(z) = J_{2n}\nabla\mathcal{H}(z)$ and $DF(z) = J_{2n}\nabla^2\mathcal{H}(z)$. Since $\nabla^2\mathcal{H}$ is continuous and the trajectory remains in K , we have

$$\|DF(\Phi^t(x))\|_2 = \|J_{2n}\nabla^2\mathcal{H}(\Phi^t(x))\|_2 \leq \|\nabla^2\mathcal{H}(\Phi^t(x))\|_2 \leq L_K$$

for all $t \in [0, \Delta T]$ (using $\|J_{2n}\|_2 = 1$). Grönwall's inequality then yields

$$\|\mathbf{Y}(\Delta T; x) - I_{2n}\|_2 \leq e^{L_K \Delta T} - 1.$$

If $\Delta T < \log(2)/L_K$ (or for all ΔT if $L_K = 0$), then $e^{L_K \Delta T} - 1 < 1$.

Write

$$\mathbf{Y}(\Delta T; x) = \begin{pmatrix} \mathbf{A} & \mathbf{B} \\ \mathbf{C} & \mathbf{D} \end{pmatrix},$$

and define $E := \begin{pmatrix} 0 \\ I_n \end{pmatrix} \in \mathbb{R}^{2n \times n}$. Then

$$\mathbf{D} - I_n = E^\top (\mathbf{Y}(\Delta T; x) - I_{2n}) E,$$

so

$$\|\mathbf{D} - I_n\|_2 = \|E^\top (\mathbf{Y}(\Delta T; x) - I_{2n}) E\|_2 \leq \|E^\top\|_2 \|\mathbf{Y}(\Delta T; x) - I_{2n}\|_2 \|E\|_2 \leq \|\mathbf{Y}(\Delta T; x) - I_{2n}\|_2 < 1,$$

since $\|E\|_2 = \|E^\top\|_2 = 1$. Hence $\mathbf{D} = I_n + (\mathbf{D} - I_n)$ is invertible by the Neumann series.

Invertibility of the lower-right block $\mathbf{D}(\Delta T; x)$ implies that, near x , the map

$$(q, p) \mapsto (q, \mathbf{P}(q, p; \Delta T))$$

is a local diffeomorphism (its Jacobian is block upper-triangular with diagonal blocks I_n and \mathbf{D}). Thus, on any simply connected (q, P) -chart intersecting K , the assumptions of Theorem 3 are satisfied. Consequently, there exists a generating function $S(q, P)$ such that, viewing p and Q as functions of (q, P) ,

$$\mathbf{p}(q, P) = \partial_q S(q, P), \quad \mathbf{Q}(q, P) = \partial_P S(q, P),$$

and the generating-function identity from Theorem 3 holds for all $x \in K$ and all $0 \leq \Delta T < \Delta T_K^*$. The bounds are uniform in $x \in K$ because L_K was defined as a supremum over the compact set K . \square

Remark 1. For a Hamiltonian system $\dot{x} = J_{2n} \nabla \mathcal{H}(x)$ the Hamiltonian is conserved, i.e., $\mathcal{H}(\Phi^t(x_0)) = \mathcal{H}(x_0)$ for all t in the interval of existence. Thus any sublevel set

$$K_E := \{x \in \mathbb{R}^{2n} : \mathcal{H}(x) \leq E\}$$

is forward (and backward) invariant: if $x_0 \in K_E$, then $\mathcal{H}(\Phi^t(x_0)) = \mathcal{H}(x_0) \leq E$ for all t , hence $\Phi^t(x_0) \in K_E$. Theorem 4 is applicable when K_E is also compact, which for example holds under the following common conditions:

- (a) **Radially unbounded Hamiltonian.** If $\mathcal{H}(x) \rightarrow \infty$ as $\|x\|_2 \rightarrow \infty$, then every sublevel set K_E is compact. Hence K_E is a compact invariant set and the theorem applies. This situation is typical for mechanical systems of the form

$$\mathcal{H}(q, p) = \frac{1}{2} p^\top M(q)^{-1} p + V(q),$$

where $M(q)$ is uniformly positive definite and bounded, i.e., there exist $0 < m_* \leq m^* < \infty$ such that $M(q) - m_* I_n$ and $m^* I_n - M(q)$ are positive definite for all q , and $V(q) \rightarrow \infty$ as $\|q\|_2 \rightarrow \infty$.

- (b) **Bounded configuration space.** If the system can only move inside a bounded region $\mathcal{Q} \subset \mathbb{R}^n$ (e.g., due to constraints, periodicity, or walls) and $M(q)$ is uniformly positive definite and bounded on \mathcal{Q} , then for any energy level E the set

$$K_E \cap (\mathcal{Q} \times \mathbb{R}^n)$$

is compact and invariant under the flow.

Lastly, we demonstrate that, in the quadratic case, a generating function exists for almost every $\Delta T > 0$, thereby removing the step-size restriction.

Theorem 5 (Existence of a global generating function for quadratic \mathcal{H}). *Let $\mathcal{H}(x) = \frac{1}{2} x^\top H x$ with a symmetric matrix $H = H^\top \in \mathbb{R}^{2n \times 2n}$ and*

$$\Phi^{\Delta T}(x) = M(\Delta T)x, \quad M(\Delta T) := e^{\Delta T J_{2n} H} = \begin{pmatrix} A(\Delta T) & B(\Delta T) \\ C(\Delta T) & D(\Delta T) \end{pmatrix}.$$

Define the resonance set

$$\mathcal{R} := \{\Delta T \in \mathbb{R} : \det D(\Delta T) = 0\}.$$

Then \mathcal{R} is discrete (it has no finite accumulation point). For any $\Delta T \notin \mathcal{R}$, the hypotheses of Theorem 3 hold globally with $U = \Omega = \mathbb{R}^{2n}$ and $W = \mathbb{R}^{2n}$, and there exists a generating function $S \in C^1(\mathbb{R}^{2n})$ such that, viewing p and Q as functions of (q, P) ,

$$\mathbf{p}(q, P) = \partial_q S(q, P), \quad \mathbf{Q}(q, P) = \partial_P S(q, P),$$

and the generating-function identity from Theorem 3 holds on all of \mathbb{R}^{2n} .

Proof. The map $\Delta T \mapsto M(\Delta T)$ is real-analytic, being a matrix exponential of $\Delta T J_{2n} H$. Hence each block $A(\Delta T), B(\Delta T), C(\Delta T), D(\Delta T)$ is real-analytic in ΔT , and so is

$$f(\Delta T) := \det D(\Delta T).$$

We have $M(0) = I_{2n}$, so $D(0) = I_n$ and therefore $f(0) = 1 \neq 0$. Thus f is not identically zero, and by the identity theorem for real-analytic functions its zero set is discrete in \mathbb{R} . This proves that $\mathcal{R} = \{\Delta T : f(\Delta T) = 0\}$ is discrete.

Now fix $\Delta T \notin \mathcal{R}$. Then $D(\Delta T)$ is invertible. Since

$$\Phi^{\Delta T}(q, p) = (Q, P) = (A(\Delta T)q + B(\Delta T)p, C(\Delta T)q + D(\Delta T)p),$$

we have

$$\mathbf{P}(q, p; \Delta T) = C(\Delta T)q + D(\Delta T)p.$$

The map

$$\Psi : \mathbb{R}^{2n} \rightarrow \mathbb{R}^{2n}, \quad \Psi(q, p) := (q, \mathbf{P}(q, p; \Delta T)) = (q, C(\Delta T)q + D(\Delta T)p),$$

is linear with Jacobian

$$D\Psi(q, p) = \begin{pmatrix} I_n & 0 \\ C(\Delta T) & D(\Delta T) \end{pmatrix},$$

which is invertible because $D(\Delta T)$ is invertible. Consequently, Ψ is a global diffeomorphism $\mathbb{R}^{2n} \rightarrow \mathbb{R}^{2n}$, and $W := \Psi(\mathbb{R}^{2n}) = \mathbb{R}^{2n}$ is simply connected. Thus both conditions (i) and (ii) of Theorem 3 are satisfied with $U = \Omega = \mathbb{R}^{2n}$ and $W = \mathbb{R}^{2n}$.

By Theorem 3 there exists $S \in C^1(\mathbb{R}^{2n})$, unique up to an additive constant, such that, when we express p and Q as functions of (q, P) via

$$(q, P) = \Psi(q, p), \quad (Q, P) = \Phi^{\Delta T}(q, p),$$

we have

$$\mathbf{p}(q, P) = \partial_q S(q, P), \quad \mathbf{Q}(q, P) = \partial_P S(q, P),$$

and the associated generating function $S^{\Delta T}$ satisfies the generating-function identity from Theorem 3 on all of \mathbb{R}^{2n} . \square

In summary, this section derives verifiable conditions ensuring that the mixed flow increment (14) admits a type-II generating function $S^{\Delta T}$ on the mixed-data domain Ω , thereby justifying the RKHS target assumption and enabling the convergence analysis from the previous section to apply.

4 Numerical Experiments

We evaluate the proposed symplectic kernel predictor on benchmark Hamiltonian systems and compare it against a structure-preserving baseline. As a high-fidelity reference we use the implicit midpoint rule with a sufficiently small micro time step $\Delta t = 10^{-3}$. We report two error measures:

(i) maximum residual error versus number of centers. Let s_m denote the surrogate after m steps of the greedy procedure, and let $e_m := u - s_m$ be the corresponding interpolation error of the target potential u . For the training and validation input sets X_{train} and X_{val} , we report, for $X \in \{X_{\text{train}}, X_{\text{val}}\}$, the discrete uniform norm of the gradient residual

$$E_X(m) := \max_{\ell \in \mathcal{J}} \max_{x \in X} |\partial_\ell e_m(x)|,$$

i.e., the worst-case gradient mismatch over X as a function of the number of selected centers m .

(ii) Relative error over time. At multiples of the macro time step $t_k = k\Delta T \in \mathbb{T}_{\Delta T}$ we quantify the deviation from the reference trajectory by

$$e_{\text{rel}}(t_k) := \frac{\|x_{\text{pred}}(t_k) - x_{\text{ref}}(t_k)\|_2}{\|x_{\text{ref}}(t_k)\|_2},$$

where $x_{\text{ref}}(t_k)$ denotes the reference solution obtained with the micro-step implicit midpoint scheme, and $x_{\text{pred}}(t_k)$ is the state obtained from the symplectic kernel predictor at time t_k .

Both the kernel and its shape parameter are selected by minimizing the error on the validation set: among a grid of shape parameters $\varepsilon > 0$ and the kernels listed below, we choose the pair (kernel,

ε) that minimizes the validation objective (here, $E_{X_{\text{val}}}(m^*)$ for a fixed m^*). We consider radial kernels of the form $k(x, x'; \varepsilon) = \kappa(\varepsilon r)$ with $r = \|x - x'\|_2$, including the inverse multiquadric (IMQ) kernel, Gaussian, linear Matérn, and quadratic Matérn kernels:

$$\begin{aligned} \text{IMQ: } \kappa_{\text{IMQ}}(r; \varepsilon) &= \frac{1}{\sqrt{1 + (\varepsilon r)^2}}, \\ \text{Gaussian: } \kappa_{\text{G}}(r; \varepsilon) &= \exp(-(\varepsilon r)^2), \\ \text{Matérn-}\frac{3}{2} \text{ ("linear" Matérn): } \kappa_{\text{M1}}(r; \varepsilon) &= (1 + \varepsilon r) \exp(-\varepsilon r), \\ \text{Matérn-}\frac{5}{2} \text{ ("quadratic" Matérn): } \kappa_{\text{M2}}(r; \varepsilon) &= (1 + \varepsilon r + \frac{1}{3}(\varepsilon r)^2) \exp(-\varepsilon r). \end{aligned}$$

4.1 Pendulum

We first consider the mathematical pendulum with Hamiltonian

$$\mathcal{H}(q, p) = \frac{p^2}{2ml^2} + mgl(1 - \cos q), \quad m = l = 1, \quad g = 9.81,$$

so that $\mathcal{H}(q, p) = \frac{1}{2}p^2 + g(1 - \cos q)$ and choose a final time $T = 6.0$. We define the box

$$\hat{\Omega} := [-\pi, \pi] \times [-2\sqrt{g}, 2\sqrt{g}],$$

and the energy-bounded domain

$$\Omega := \left\{ (q, p) \in \hat{\Omega} : \mathcal{H}(q, p) < 2g \right\}.$$

For each initial state $x_0 = (q_0, p_0)$ we compute the reference solution $x(\cdot; x_0)$ with the implicit midpoint rule using the micro time step $\Delta t = 10^{-3}$. As a structure-preserving baseline for large steps we apply the implicit midpoint rule directly with the macro step ΔT .

We consider two cases that differ in the sampling scenario. In both cases, we first create a uniform tensor-product grid X on $\hat{\Omega}$ with 200×200 points and retain only those inside the energy-bounded set Ω . We then define the training sets

$$\mathcal{M}_A^{\Delta T} := \left\{ \left(I_1 x_0 + I_2 \Phi^{\Delta T}(x_0), J_{2n}^\top \frac{\Phi^{\Delta T}(x_0) - x_0}{\Delta T} \right) : x_0 \in X \cap \Omega \right\},$$

and

$$\mathcal{M}_B^{\Delta T} := \left\{ \left(I_1 x_0 + I_2 \Phi^{\Delta T}(x_0), J_{2n}^\top \frac{\Phi^{\Delta T}(x_0) - x_0}{\Delta T} \right) : x_0 \in X \cap \Omega^- \right\},$$

with

$$\Omega^- := \left\{ (q, p) \in \Omega : p \leq 0 \right\}.$$

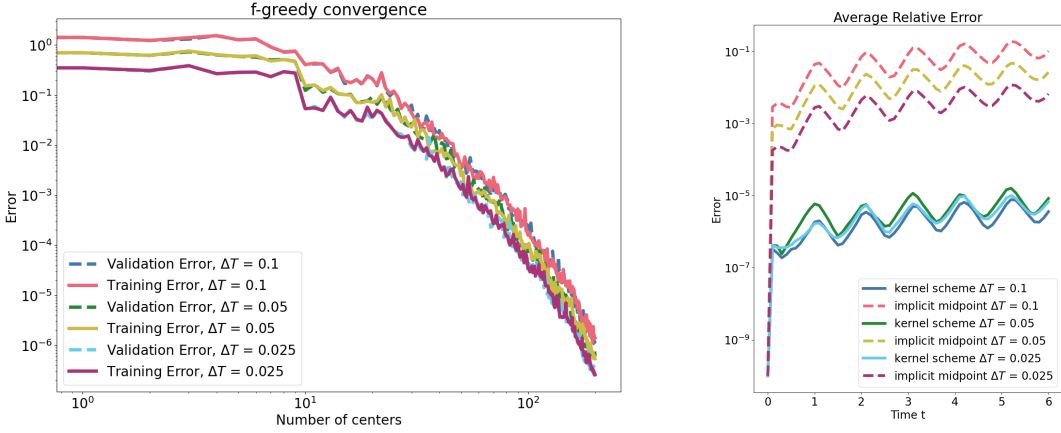
In both cases, $x(\Delta T; x_0)$ is approximated using the implicit midpoint rule with the micro time step Δt .

For testing, we draw 10 initial conditions with $q_0 \sim \mathcal{U}([0, \pi])$ and $p_0 = 0$, and evolve each trajectory up to $T = 6.0$ using (i) the proposed symplectic predictor, (ii) the implicit midpoint rule with step ΔT , and (iii) the reference micro-step solution (time step Δt). Note that

$$\nabla^2 \mathcal{H}(q, p) = \begin{pmatrix} 9.81 \cos q & 0 \\ 0 & 1 \end{pmatrix}, \quad L_K := \sup_{(q, p) \in K} \|\nabla^2 \mathcal{H}(q, p)\|_2 \leq 9.81,$$

so that

$$\Delta T_K^* = \min \left\{ T, \frac{\log 2}{9.81} \right\} \approx 7.07 \times 10^{-2}.$$



(a) f -greedy interpolation error versus the number of selected centers for three macro time step sizes, showing training (solid) and validation (dashed) curves. (b) Relative error over time comparing the symplectic kernel scheme (solid) with the implicit-midpoint baseline (dashed) for three macro time step sizes.

Figure 2: Pendulum: (a) f -greedy convergence vs. centers; (b) relative error over time.

Hence, the hypotheses of Theorem 4 are guaranteed for $\Delta T < 7.07 \times 10^{-2}$, implying existence of a generating function; since the underlying Grönwall-type estimate is conservative, we test $\Delta T \in \{0.1, 0.05, 0.025\}$, including a regime with $\Delta T > \Delta T_K^*$.

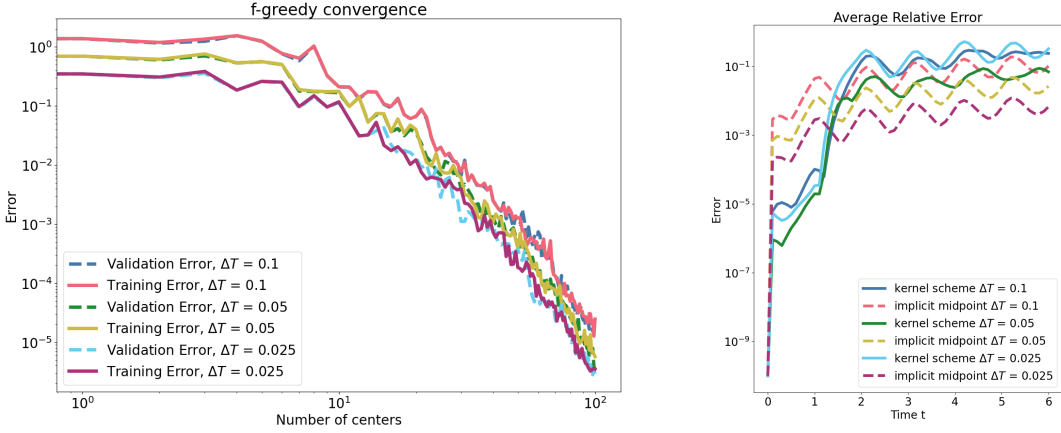
As a first numerical result, we present the convergence of the greedy procedure in Figure 2a. For $\Delta T \in \{0.1, 0.05, 0.025\}$, we report the maximum residual error as a function of the number of centers both for training and validation data. After a short plateau (for roughly the first 15 centers), all curves exhibit an almost straight-line decay on the log–log axes, i.e., an approximately algebraic convergence, reaching values of order $\sim 10^{-6}$ by about 200 centers. Training and validation errors track closely for all ΔT , with the validation error slightly above the training error, indicating good generalization and no visible overfitting. Moreover, the error decay for smaller ΔT starts from a slightly lower level and attains a slightly lower minimal error.

Next, we apply the kernel scheme to predict the 10 trajectories corresponding to the 10 randomly chosen initial conditions described above, and present the average relative error. The results are shown in Figure 2b. Over the entire time horizon, the kernel scheme achieves errors between $\sim 10^{-7}$ and $\sim 10^{-5}$. The implicit-midpoint curves are 3–4 orders of magnitude larger at the same ΔT , rising from $\sim 10^{-3}$ to $\sim 10^{-1}$ while displaying similar oscillations. Decreasing ΔT uniformly lowers all implicit-midpoint curves (best for $\Delta T = 0.025$, then 0.05, then 0.1); however, the kernel predictor remains more accurate for every step size. In contrast and remarkably, even though the kernel scheme exhibits slightly faster convergence for smaller ΔT , it performs best for the largest ΔT , likely due to the smaller number of macro steps required to span the trajectory, which reduces error accumulation.

Next, we show the same experiment, but with a reduced training set $\mathcal{M}_B^{\Delta T}$. We reduce the maximum number of centers by a factor of 1/2, yielding a fill distance comparable to that in the previous experiment with the larger domain.

In Figure 3a we report the maximum residual error as a function of the number of centers for $\Delta T \in \{0.1, 0.05, 0.025\}$. The decay is very similar to the original experiment with the larger training set.

In Figure 3b, the relative error is shown, averaged over the same 10 random initial conditions. Over



(a) f -greedy interpolation error versus the number of selected centers for three macro time step sizes, showing training (solid) and validation (dashed) curves.

(b) Relative error over time comparing the symplectic kernel scheme (solid) with the implicit-midpoint baseline (dashed) for three macro time step sizes.

Figure 3: Pendulum (reduced training set): (a) f -greedy convergence vs. centers; (b) relative error over time.

the horizon $T = 6$, the kernel scheme starts with very small errors (about 10^{-7} – 10^{-5} near $t \approx 0$) but then these increase as the trajectory leaves the training domain at $t = \pi\sqrt{l/g} \approx 1.00$ and the error settles between 10^{-2} and 10^{-1} , growing only mildly over time. Beyond the training horizon ($t \approx 1.00$), the error of the symplectic kernel predictor remains bounded, with the small oscillations typical of symplectic schemes. For $\Delta T = 0.05$, its accuracy is comparable to that of the implicit midpoint scheme with $\Delta T = 0.1$ up to $T = 6$. Note that these results still consistently indicate very good performance of all the symplectic schemes, as a non-symplectic integrator, e.g., explicit Euler often produces relative error several orders of magnitude larger than 100% [2, 33, 34, 35]. To highlight the generalization capabilities, in Figure 4 we compare one pendulum trajectory obtained from the kernel scheme (solid blue, $\Delta T = 0.025$) with the reference solution (orange dashed), for both the angle $q(t)$ (top panel) and the angular momentum $p(t)$ (bottom panel). The two curves

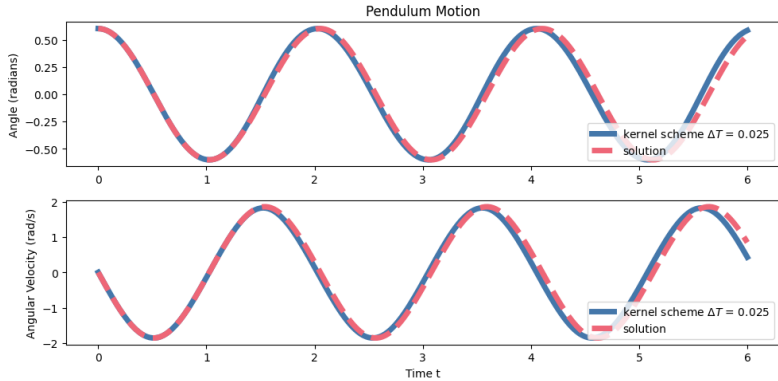


Figure 4: Pendulum generalization test: comparison of one trajectory obtained from the kernel scheme ($\Delta T = 0.025$) with the reference solution.

almost coincide over the entire time interval, demonstrating very good generalization beyond the training domain: the amplitudes and qualitative shape of the oscillations are preserved, and no spurious growth or unphysical behavior is observed. The remaining discrepancy is dominated by a slight phase shift between predictor and reference, rather than by an incorrect or nonphysical trajectory.

4.2 Nonlinear spring–mass chain with fixed ends

We next consider a nonlinear spring–mass chain, that is, a row of point masses connected by springs between two fixed walls. Let $n \in \mathbb{N}$ point masses be arranged on a line with displacements

$$q = (q_1, \dots, q_n)^\top$$

that are measured from the equilibrium configuration, momenta

$$p = (p_1, \dots, p_n)^\top,$$

and mass matrix $M = \text{diag}(m_1, \dots, m_n)$. In the experiments below we take $m_1 = \dots = m_n = 1$, so that $p = M\dot{q} = \dot{q}$. Fixed ends are enforced via virtual nodes $q_0 \equiv 0$ and $q_{n+1} \equiv 0$. The spring elongations are given by

$$\delta_i(q) := q_{i+1} - q_i, \quad i = 0, \dots, n,$$

which can be written compactly as $\delta = Bq$ with

$$B = \begin{bmatrix} 1 & 0 & 0 & \cdots & 0 \\ -1 & 1 & 0 & \cdots & 0 \\ 0 & -1 & 1 & \ddots & \vdots \\ \vdots & \ddots & \ddots & \ddots & 0 \\ 0 & \cdots & 0 & -1 & 1 \\ 0 & \cdots & \cdots & 0 & -1 \end{bmatrix} \in \mathbb{R}^{(n+1) \times n},$$

so that

$$(Bq)_0 = q_1, \quad (Bq)_i = q_{i+1} - q_i \quad (1 \leq i \leq n-1), \quad (Bq)_n = -q_n,$$

and hence $Bq = (\delta_0, \dots, \delta_n)^\top$.

Given C^1 spring potentials $f_i : \mathbb{R} \rightarrow \mathbb{R}$ and

$$\sigma(z) := (f'_0(z_0), \dots, f'_n(z_n))^\top, \quad z = (z_i)_{i=0}^n \in \mathbb{R}^{n+1},$$

the potential energy and its gradient are

$$V(q) = \sum_{i=0}^n f_i((Bq)_i), \quad \nabla_q V(q) = B^\top \sigma(Bq).$$

We consider identical quartic spring potentials of the form

$$f_i(\delta_i) = \frac{1}{2}\alpha\delta_i^2 + \frac{\beta}{4}\delta_i^4, \quad \sigma_i(\delta_i) = f'_i(\delta_i) = \alpha\delta_i + \beta\delta_i^3,$$

with parameters $\alpha = 1$ and $\beta = 0.25$ for all $i = 0, \dots, n$. In the absence of damping, the equations of motion read

$$M\ddot{q} + B^\top \sigma(Bq) = 0.$$

Introducing the state $x = (q, p)$ and the Hamiltonian

$$\mathcal{H}(q, p) = \frac{1}{2}p^\top M^{-1}p + V(q),$$

we obtain the canonical Hamiltonian system

$$\dot{x} = J_{2n} \nabla H(x),$$

with the standard symplectic matrix J_{2n} . In the numerical experiments below we fix $n = 3$. We study two training scenarios that differ in the sampling of initial conditions. In both cases we first draw candidate states from a bounded box and retain only those below a prescribed energy level. Specifically, let

$$\hat{\Omega} = ([-q_{\max}, q_{\max}]^n \times [-p_{\max}, p_{\max}]^n) \subset \mathbb{R}^{2n}, \quad q_{\max} = 0.5, \quad p_{\max} = 0.5,$$

and define the energy-bounded subset

$$\Omega = \left\{ (q, p) \in \hat{\Omega} : \mathcal{H}(q, p) \leq H_{\max} \right\}, \quad \mathcal{H}(q, p) = \frac{1}{2} p^T M^{-1} p + \sum_{i=0}^n f_i(\delta_i(q)), \quad H_{\max} = 0.5.$$

We generate states

$$(q^{(j)}, p^{(j)}) \sim \mathcal{U}(\hat{\Omega}),$$

and retain only those satisfying the energy constraint:

$$X = \left\{ (q^{(j)}, p^{(j)}) \in \hat{\Omega} : H(q^{(j)}, p^{(j)}) \leq H_{\max} \right\} \subset \Omega$$

until $N_s = 10000$ states have been collected.

The training data for scenario A are defined as

$$\mathcal{M}_A^{\Delta T} := \left\{ \left(I_1 x_0 + I_2 \Phi^{\Delta T}(x_0), J_{2n}^T \frac{\Phi^{\Delta T}(x_0) - x_0}{\Delta T} \right) : x_0 \in X \right\},$$

that is, pairs of states at times 0 and ΔT along trajectories starting from $x_0 \in X$. In scenario B, we restrict the initial conditions to a half-space in momentum,

$$\Omega^- = \{ (q, p) \in \Omega : p_2 \leq 0 \},$$

and construct

$$\mathcal{M}_B^{\Delta T} := \left\{ \left(I_1 x_0 + I_2 \Phi^{\Delta T}(x_0), J_{2n}^T \frac{\Phi^{\Delta T}(x_0) - x_0}{\Delta T} \right) : x_0 \in X \cap \Omega^- \right\}.$$

In both cases, $x(\Delta T; x_0)$ is approximated by the implicit midpoint rule with micro time step Δt . For evaluation we draw 10 test initial conditions independently of the training data according to

$$q_0 \sim \mathcal{U}([0, q_{\max}]^3), \quad p_0 = 0,$$

and integrate each test trajectory up to $T = 10.0$ using (i) the proposed symplectic kernel predictor, (ii) the implicit midpoint method with macro time step ΔT , and (iii) a high-fidelity reference solution obtained by the implicit midpoint rule with micro time step Δt .

Note, that we have

$$\nabla^2 \mathcal{H}(q, p) = \begin{pmatrix} B^T \text{diag} \left(1 + 3\beta (Bq)_i^2 \right)_{i=0}^n B & 0 \\ 0 & I_n \end{pmatrix}, \quad L_K \leq \max \{ 1, \|B\|_2^2 (1 + 3\beta \delta_K^2) \},$$

with $\delta_K := \sup_{(q, p) \in K} \|Bq\|_{\infty}$. For $n = 3$ and $q_i \in [-0.5, 0.5]$, each elongation is a difference of two coordinates (or a boundary value),

$$\delta_0 = q_1, \quad \delta_1 = q_2 - q_1, \quad \delta_2 = q_3 - q_2, \quad \delta_3 = -q_3,$$

hence $|\delta_i| \leq 1$ for all i and therefore $\delta_K = \sup_{(q,p) \in K} \|Bq\|_\infty \leq 1$. Moreover,

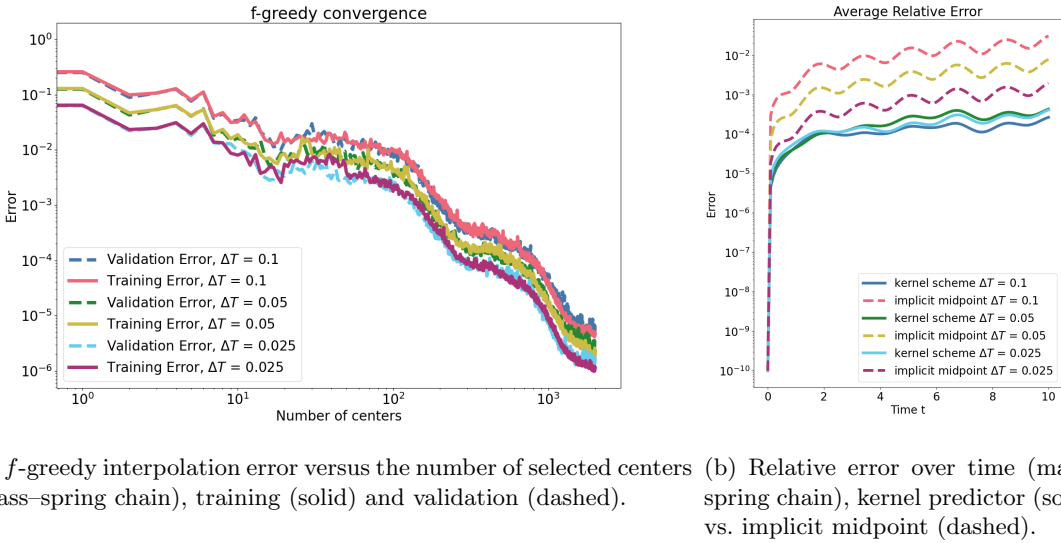
$$\|B\|_2^2 = \|B^\top B\|_2 = \lambda_{\max}(B^\top B).$$

Since $B^\top B$ is tridiagonal with diagonal entries 2 and off-diagonals -1 , the Gershgorin circle theorem yields $\sigma(B^\top B) \subset [0, 4]$, hence

$$\|B^\top B\|_2 = \lambda_{\max}(B^\top B) \leq 4 \quad \text{and} \quad \|B\|_2^2 \leq 4.$$

Therefore,

$$L_K \leq 4 \left(1 + \frac{3}{4}\right) = 7, \quad \Delta T_K^* = \min \left\{ T, \frac{\log 2}{L_K} \right\} \geq \frac{\log 2}{7} \approx 9.90 \times 10^{-2}.$$



(a) f -greedy interpolation error versus the number of selected centers (mass–spring chain), training (solid) and validation (dashed).

(b) Relative error over time (mass–

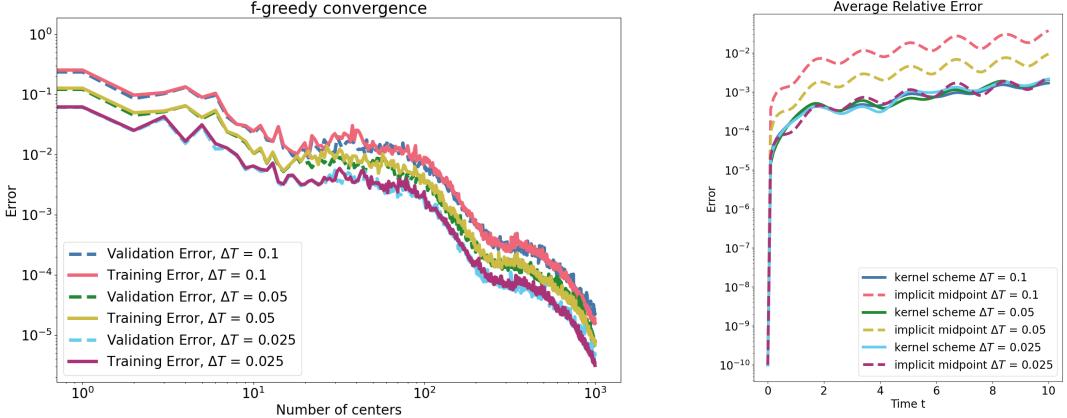
(mass–spring chain), kernel predictor (solid) vs. implicit midpoint (dashed).

Figure 5: Mass–spring chain: (a) f -greedy convergence vs. centers; (b) relative error over time.

As a first numerical result we report in Figure 5a the convergence of the greedy center selection. The maximum residual error is shown as a function of the number of centers m for $\Delta T \in \{0.1, 0.05, 0.025\}$. For all three macro time steps, the error decreases steadily from approximately 10^{-1} to about 10^{-3} around $m \approx 10^2$, and reaches values close to 10^{-6} by $m \approx 10^3$. Training and validation curves are very close over the entire range of m , with the validation error only slightly above the training error, indicating good generalization and no apparent overfitting. As in the previous examples, smaller macro time steps yield slightly lower error levels, but the qualitative decay behavior is essentially the same for all ΔT .

We then apply the kernel scheme to the 10 test trajectories and show the average relative error in Figure 5b. Over the full time interval $[0, 10]$, the kernel predictor achieves errors between approximately 10^{-5} and a few $\times 10^{-4}$, with only mild temporal oscillations. The structure-preserving baseline (implicit midpoint with step size ΔT) is systematically less accurate: its error ranges from about 10^{-3} to a few $\times 10^{-2}$, i.e., typically one to almost two orders of magnitude larger than that of the kernel predictor at the same ΔT , while displaying a similar oscillatory pattern. Reducing ΔT lowers all implicit-midpoint curves as expected, but the kernel predictor remains more accurate for every step size and throughout the entire time interval.

We next repeat the experiment with the reduced training set $\mathcal{M}_B^{\Delta T}$ (and a maximum of 1000 centers); see Figures 6a and 6b.



(a) f -greedy interpolation error versus the number of selected centers (mass–spring chain, reduced training set), training (solid) and validation (dashed).

(b) Relative error over time (mass–spring chain, reduced training set), kernel predictor (solid) vs. implicit midpoint (dashed).

Figure 6: Mass–spring chain (reduced training set): (a) f -greedy convergence vs. centers; (b) relative error over time.

In Figure 6a, the maximum residual error again decreases monotonically with the number of centers for all $\Delta T \in \{0.1, 0.05, 0.025\}$. The curves start between approximately 10^{-1} and 3×10^{-1} and drop to the 10^{-3} level around $m \approx 100$, reaching about 10^{-6} by $m \approx 10^3$. Training and validation errors remain close throughout the range of m , with the validation curves only slightly above the training curves, again indicating good generalization and no visible overfitting. As before, smaller macro time steps yield lower error levels, but the decay behavior is essentially identical for all three ΔT .

In Figure 6b, the average relative error over 10 random initial conditions remains well controlled on $[0, 10]$, with the kernel scheme achieving errors between roughly 10^{-5} and 10^{-3} depending on ΔT . The implicit-midpoint baseline is consistently less accurate, with errors between about 10^{-4} and a few $\times 10^{-2}$, i.e., typically one to almost two orders of magnitude larger at matched ΔT , while again exhibiting similar oscillatory patterns. The kernel predictor generalizes well along the entire trajectories: its error does not exhibit uncontrolled growth and remains below the baseline for most of the time. For each ΔT , the kernel scheme is approximately as accurate as the implicit midpoint rule with the smallest macro time step $\Delta T = 0.025$ over the full interval up to $T = 10$. The generalization experiment for the spring–mass chain (training on $\Omega^- = \{(q, p) \in \Omega : p_2 \leq 0\}$ and testing on $p_2 > 0$) performs almost as well as the fully sampled case. This behavior can be related to the mechanical Hamiltonian structure $\mathcal{H}(q, p) = \frac{1}{2}p^\top M^{-1}p + V(q)$, which depends on p only through the quadratic kinetic energy and is therefore invariant under $p \mapsto -p$. The associated Hamiltonian vector field changes sign when p is reversed. Consequently, the “unseen” half-space $\{p_2 > 0\}$ essentially contains the same trajectories as $\{p_2 < 0\}$, traversed with opposite momentum. In addition, the symplectic Euler argument $\xi_j = (q_0^{(j)}, p_{\Delta T}^{(j)})$ already contains many samples with positive $p_{\Delta T, 2}$ even when $p_{0, 2} \leq 0$, and the learning targets are difference quotients of this sign-reversing vector field. Combined with the weakly nonlinear, small-amplitude regime considered here, these symmetries make extrapolation across $p_2 = 0$ comparatively benign and help explain the strong generalization performance.

4.3 Discretized wave equation

We consider the one-dimensional wave equation on a finite interval. For time $t \in I = (0, T)$ and spatial variable $\xi \in \Omega := (0, L)$, find $u : \bar{I} \times \bar{\Omega} \rightarrow \mathbb{R}$ such that

$$\begin{aligned} u_{tt}(t, \xi) &= c^2 u_{\xi\xi}(t, \xi) && \text{in } I \times \Omega, \\ u(t, \xi) &= 0 && \text{on } I \times \partial\Omega, \\ u(0, \xi) &= u_0(\xi), \quad u_t(0, \xi) = v_0(\xi) && \text{in } \Omega, \end{aligned}$$

with wave speed $c = 0.3$ domain length $L = 1$ and end time $T = 6$ in the numerical experiments. We discretize Ω by a uniform grid $\{\xi_i\}_{i=1}^N \subset (0, L)$ with $N = 1000$ and enforce homogeneous Dirichlet data at $\xi = \{0, L\}$. Let $D_{\xi\xi} \in \mathbb{R}^{N \times N}$ be the standard (symmetric positive definite) central-difference matrix for $-\partial_{\xi\xi}$ with homogeneous Dirichlet boundaries. With $u(t) \in \mathbb{R}^N$ the vector of nodal values, the semi-discrete equation reads

$$\ddot{u}(t) = -c^2 D_{\xi\xi} u(t).$$

Introduce the phase-space state

$$x(t) = \begin{bmatrix} q(t) \\ p(t) \end{bmatrix} = \begin{bmatrix} u(t) \\ \dot{u}(t) \end{bmatrix} \in \mathbb{R}^{2N},$$

and the quadratic Hamiltonian

$$\mathcal{H}(x) = \frac{1}{2} p^\top p + \frac{1}{2} c^2 q^\top D_{\xi\xi} q.$$

Then the dynamics take canonical Hamiltonian form

$$\dot{x}(t) = J_{2N} \nabla_x \mathcal{H}(x(t)) = J_{2N} H x(t), \quad J_{2N} = \begin{bmatrix} 0 & I_N \\ -I_N & 0 \end{bmatrix},$$

with the symmetric matrix

$$H = \begin{bmatrix} c^2 D_{\xi\xi} & 0 \\ 0 & I_N \end{bmatrix}, \quad x(0) = [u_0(\xi_1), \dots, u_0(\xi_N), v_0(\xi_1), \dots, v_0(\xi_N)]^\top.$$

Note that, since \mathcal{H} is quadratic, the hypotheses of Theorem 5 apply; consequently, a (global) generating function exists for all step sizes ΔT outside a discrete resonance set.

To compress the $2N$ -dimensional Hamiltonian system while preserving structure, we use symplectic model order reduction [36, 37, 38] to project onto a symplectic subspace spanned by $V \in \mathbb{R}^{2N \times 2n}$, $n \ll N$, satisfying $V^\top J_{2N} V = J_{2n}$. Reduced coordinates are obtained with the symplectic inverse

$$x_{\text{red}}(t) = V^+ x(t), \quad V^+ := J_{2n}^\top V^\top J_{2N}, \quad x(t) \approx V x_{\text{red}}(t).$$

For the quadratic Hamiltonian $\mathcal{H}(x) = \frac{1}{2} x^\top H x$ the reduced Hamiltonian is

$$\mathcal{H}_{\text{red}}(x_{\text{red}}) = \frac{1}{2} x_{\text{red}}^\top (V^\top H V) x_{\text{red}},$$

and the reduced dynamics remain a canonical Hamiltonian system:

$$\dot{x}_{\text{red}}(t) = J_{2n} \nabla_{x_{\text{red}}} \mathcal{H}_{\text{red}}(x_{\text{red}}) = J_{2n} (V^\top H V) x_{\text{red}}(t), \quad x_{\text{red}}(0) = V^+ x(0).$$

In practice, we construct V via the complex SVD (cSVD): collect snapshots $Q = [q(t_k)]$ and $P = [p(t_k)]$, form the complex snapshot matrix $Y := Q + iP$, compute the thin SVD $Y \approx U \Sigma W^*$, and set

$$V = \begin{bmatrix} \text{Re } U & -\text{Im } U \\ \text{Im } U & \text{Re } U \end{bmatrix}.$$

This yields a structure-preserving reduced-order model that conserves the quadratic energy and inherits the stability properties of the full system.

In this experiment we do not sample (q, p) from a hypercube. Instead, we assemble initial conditions from single sine modes with unit amplitude. Let

$$B := 2, \quad \mathcal{N} := \{1, \dots, B\}.$$

On the Dirichlet grid $\xi_i = ih$ with $h = L/(N + 1)$ ($i = 1, \dots, N$), define the discrete sine vectors

$$\Phi_n := (\sin(n\pi\xi_i/L))_{i=1}^N \in \mathbb{R}^N, \quad n \in \mathcal{N}.$$

We introduce an enumeration $\{(a_j, b_j)\}_{j=1}^{B^2} := \mathcal{N} \times \mathcal{N}$. For each pair we set

$$q_0^{(j)} = \Phi_{a_j}, \quad p_0^{(j)} = \Phi_{b_j}, \quad x_0^{(j)} := \begin{bmatrix} q_0^{(j)} \\ p_0^{(j)} \end{bmatrix} \in \mathbb{R}^{2N}, \quad j = 1, \dots, B^2.$$

We assemble the phase-space snapshot matrix

$$X := \left[x_0^{(1)}, \dots, x_0^{(B^2)} \right] \in \mathbb{R}^{2N \times B^2},$$

and apply the cSVD procedure to X to obtain the symplectic basis $V \in \mathbb{R}^{2N \times 2n}$ as described above.

In the reduced system, we then sample initial conditions directly in the reduced phase space. More precisely, we draw

$$z_0 \sim \mathcal{U}([-z_{\max}, z_{\max}]^{2n}),$$

and define the corresponding full initial state as $x_0 = Vz_0$. We retain only those satisfying the energy constraint

$$Z_{\text{train}} = \left\{ z_0^j \in \hat{\Omega} : H(z_0^j) \leq H_{\max} \right\} \subset \Omega$$

with $H_{\max} = 5$ until $N_s = 20000$ states have been collected.

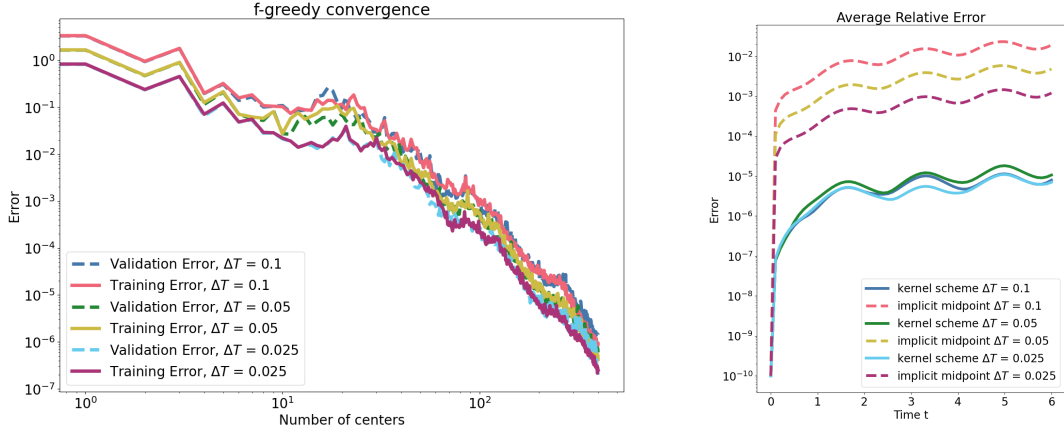
The training set for the kernel predictor is then given by

$$\mathcal{M}^{\Delta T} := \left\{ \left(I_1 z_0 + I_2 \Phi^{\Delta T}(z_0), J_{2n}^{\top} \frac{\Phi^{\Delta T}(z_0) - z_0}{\Delta T} \right) : z_0 \in Z_{\text{train}} \right\}.$$

This two-stage procedure (mode-based generation of full-order initial data, followed by cSVD-based reduction and hypercube sampling in reduced coordinates) concentrates the basis on low-frequency wave patterns while preserving flexibility in the reduced sampling used to train the kernel predictor. For testing we draw 10 test initial conditions independently of the training set, using the same mode-based sampling procedure as above. Each test trajectory is then evolved up to $T = 6.0$ using (i) the proposed symplectic kernel predictor, (ii) the implicit midpoint method with macro time step size ΔT , and (iii) a high-fidelity reference solution computed by the implicit midpoint rule with micro time step Δt .

As a first numerical result, we report in Figure 7a the convergence behavior of the f -greedy center selection.

In Figure 7a we report the maximum residual error as a function of the number of centers for $\Delta T \in \{0.1, 0.05, 0.025\}$. For all three macro time steps, the curves exhibit a short pre-asymptotic regime for small numbers of centers (up to roughly $m \approx 10$), followed by an almost straight-line decay on the log-log scale. This indicates algebraic convergence of the interpolation error over nearly three orders of magnitude: starting from values of order 10^0 – 10^1 at $m = 1$, the error drops below 10^{-3} after about $m \approx 30$ centers and reaches values close to 10^{-6} by $m \approx 300$ – 400 . Training and validation errors remain very close for all ΔT , with the validation curves lying slightly above the training curves, indicating good generalization and no overfitting. As expected, smaller macro



(a) f -greedy interpolation error versus the number of selected centers (wave model), training (solid) and validation (dashed). (b) Average relative error over time (wave model), kernel predictor (solid) vs. implicit midpoint (dashed).

Figure 7: Reduced 1D wave model: (a) f -greedy convergence vs. centers; (b) average relative error over time.

time steps yield somewhat lower error levels across the entire range of m , but the qualitative decay behavior is essentially the same for all three step sizes.

In Figure 7b we show the average relative error for the ten test trajectories over the time interval $[0, 6]$. The kernel predictor achieves errors in the range 10^{-7} – 10^{-5} : after a rapid initial increase from machine precision, the error levels off and exhibits small temporal oscillations, characteristic of symplectic updates for oscillatory systems. The three kernel curves for $\Delta T \in \{0.1, 0.05, 0.025\}$ nearly coincide, indicating that the method is robust with respect to the macro time step size in this reduced setting. In contrast, the implicit midpoint baseline with the same macro time step experiences significantly larger errors, ranging from about 10^{-3} up to roughly 10^{-1} by $t = 6$, with a clear ordering: $\Delta T = 0.1$ (largest error), $\Delta T = 0.05$, and $\Delta T = 0.025$ (smallest error). Thus, for every tested macro time step the kernel predictor reduces the error by roughly three orders of magnitude compared to the structure-preserving baseline, while maintaining stable, oscillatory error profiles over the entire time horizon.

5 Conclusion and Outlook

In this work we proposed a kernel-based surrogate model for Hamiltonian dynamics that is symplectic by construction and tailored to large time horizons. The core idea is to learn a scalar potential s whose gradient, evaluated on a mixed argument $(q_0, p_{\Delta T})$, enters an implicit symplectic-Euler update. This yields a discrete flow map that preserves the canonical symplectic structure exactly and inherits the favorable long-time behavior of symplectic integrators. By formulating the learning task as a HB interpolation problem for gradients, we can leverage the RKHS framework to construct surrogates with rigorous approximation guarantees and controlled complexity.

On the theoretical side, we established existence results for the target potential underlying the symplectic Euler mixed argument. For general Hamiltonian systems we derived conditions on the exact flow $\Phi^{\Delta T}$ under which there exists a generating function $S^{\Delta T}(q, P)$ whose gradients reproduce the discrete flow increment on a mixed $(q_0, p_{\Delta T})$ chart. These conditions can be verified locally under a step-size restriction on ΔT based on uniform invertibility of the $(q, p) \mapsto (q, P)$

mapping on compact forward-invariant sets, and globally for quadratic Hamiltonians outside a discrete resonance set. In addition, we extended existing convergence theory for greedy kernel approximation to the gradient HB setting, proving residual bounds.

On the algorithmic side, we combined the proposed symplectic kernel predictor with model order reduction (via the cSVD) to obtain a low-dimensional canonical surrogate model for a high-dimensional discretized PDE. This produces reduced models that remain Hamiltonian and energy-conserving, while significantly lowering the cost of both training and online evaluation of the kernel surrogate. In all components, the construction preserves the underlying geometric structure of the original system.

The numerical experiments on three benchmark problems—the mathematical pendulum, a nonlinear spring–mass chain with fixed ends, and a discretized wave equation with symplectic MOR—confirm the effectiveness of the proposed approach. Across all test cases, the greedy procedure produces sparse surrogates with nearly algebraic decay of the interpolation error over several orders of magnitude, and training/validation errors remain closely aligned, indicating good generalization. In long-time simulations, the symplectic kernel predictor consistently outperforms a structure-preserving baseline (implicit midpoint with the same macro step), typically reducing trajectory errors by two to three orders of magnitude while maintaining bounded, oscillatory error profiles characteristic of symplectic schemes, even in generalization settings where parts of phase space are unseen during training.

The present work focuses on learning a time- ΔT flow map for a fixed macro time step, and on kernel models with a fixed prediction horizon. An interesting direction for future research is to relax this constraint and treat the macro step size as an additional variable. One option is to learn a family of generating functions $S^{\Delta T}$ parameterized by ΔT , or to augment the input with a time parameter and equip it with a suitable kernel, thereby obtaining a single surrogate that can be evaluated for a continuum of macro step sizes. Similarly, the prediction horizon T of the kernel model can be promoted to an explicit parameter, allowing the construction of surrogates that learn the joint dependence on state and time and thus support variable-step or adaptive-in-time structure-preserving prediction. We expect such extensions to broaden the applicability of the proposed framework, in particular for problems where accuracy and efficiency requirements naturally call for adaptive macro time stepping.

Funding

Funded by Deutsche Forschungsgemeinschaft (DFG, German Research Foundation) under Germany’s Excellence Strategy – EXC 2075/2 – 390740016.

Competing interests

The authors report there are no competing interests to declare.

References

- [1] Ana Cannas da Silva. *Lectures on Symplectic Geometry*. Springer Berlin Heidelberg, Berlin, Heidelberg, 2008. ISBN 978-3-540-45330-7. doi:10.1007/978-3-540-45330-7.
- [2] Ernst Hairer, Marlis Hochbruck, Arieh Iserles, and Christian Lubich. Geometric numerical integration. *Oberwolfach Reports*, 3(1):805–882, 2006. doi:10.4171/OWR/2006/14.
- [3] Kevin T. Carlberg, Antony Jameson, Mykel J. Kochenderfer, Jeremy Morton, Liqian Peng, and Freddie D Witherden. Recovering missing CFD data for high-order discretizations us-

- ing deep neural networks and dynamics learning. *J. Comput. Phys.*, 395:105–124, 2019. doi:10.1016/j.jcp.2019.05.041.
- [4] Bernhard Schölkopf and Alexander J. Smola. *Learning with Kernels: Support Vector Machines, Regularization, Optimization, and Beyond*. The MIT Press, Cambridge, MA, 2001. doi:10.7551/mitpress/4175.001.0001.
- [5] Felix Döppel, Tizian Wenzel, Robin Herkert, Bernard Haasdonk, and Martin Votsmeier. Goal-Oriented Two-Layered Kernel Models as Automated Surrogates for Surface Kinetics in Reactor Simulations. *Chemie Ingenieur Technik*, 96:759–768, 2024. doi:10.1002/cite.202300178.
- [6] Marc Peter Deisenroth, Dieter Fox, and Carl Edward Rasmussen. Gaussian processes for data-efficient learning in robotics and control. *IEEE transactions on pattern analysis and machine intelligence*, 37(2):408–423, 2013. doi:10.1109/TPAMI.2013.218.
- [7] De-Yun Zhong, Li-Guan Wang, and Lin Bi. Implicit surface reconstruction based on generalized radial basis functions interpolant with distinct constraints. *Applied Mathematical Modelling*, 71:408–420, 2019.
- [8] Antonino La Rocca and Henry Power. A double boundary collocation hermitian approach for the solution of steady state convection–diffusion problems. *Computers & Mathematics with applications*, 55(9):1950–1960, 2008.
- [9] Stefano De Marchi, Armin Iske, and Gabriele Santin. Image reconstruction from scattered radon data by weighted positive definite kernel functions. *Calcolo*, 55(1):2, 2018.
- [10] Tobias Ehring and Bernard Haasdonk. Hermite kernel surrogates for the value function of high-dimensional nonlinear optimal control problems. *Advances in Computational Mathematics*, 50(3):36, 2024. doi:10.1007/s10444-024-10128-5.
- [11] Holger Wendland. *Scattered Data Approximation*. Cambridge Monographs on Applied and Computational Mathematics. Cambridge University Press, Cambridge, UK, 2004. doi:10.1017/CBO9780511617539.
- [12] Samuel Greydanus, Misko Dzamba, and Jason Yosinski. Hamiltonian neural networks. *Advances in Neural Information Processing Systems*, 32, 2019. doi:10.48550/arXiv.1906.01563.
- [13] Marco David and Florian Méhats. Symplectic learning for Hamiltonian neural networks. *Journal of Computational Physics*, 494:112495, 2023. ISSN 0021-9991. doi:10.1016/j.jcp.2023.112495.
- [14] Tom Bertalan, Felix Dietrich, Igor Mezić, and Ioannis G Kevrekidis. On learning Hamiltonian systems from data. *Chaos: An Interdisciplinary Journal of Nonlinear Science*, 29(12), 2019. doi:10.1063/1.5128231.
- [15] Zhengdao Chen, Jianyu Zhang, Martin Arjovsky, and Léon Bottou. Symplectic recurrent neural networks. In *International Conference on Learning Representations*, 2020. doi:10.48550/arXiv.1909.13334.
- [16] Yaofeng Desmond Zhong, Biswadip Dey, and Amit Chakraborty. Symplectic ODE-Net: Learning Hamiltonian dynamics with control. In *In International Conference on Learning Representations*, 2020. doi:10.48550/arXiv.1909.12077.
- [17] Pengzhan Jin, Zhen Zhang, Aiqing Zhu, Yifa Tang, and George Em Karniadakis. SympNets: Intrinsic structure-preserving symplectic networks for identifying Hamiltonian systems. *Neural Networks*, 132:166–179, 2020. doi:10.1016/j.neunet.2020.08.017.

- [18] Joshua William Burby, Qi Tang, and Romit Maulik. Fast neural Poincaré maps for toroidal magnetic fields. *Plasma Physics and Controlled Fusion*, 63(2):024001, 2020. doi:10.1088/1361-6587/abcbaa.
- [19] Renyi Chen and Molei Tao. Data-driven prediction of general Hamiltonian dynamics via learning exactly-symplectic maps. In *International conference on machine learning*, pages 1717–1727. PMLR, 2021. doi:10.48550/arXiv.2103.05632.
- [20] Philipp Horn, Veronica Saz Ulibarrena, Barry Koren, and Simon Portegies Zwart. A generalized framework of neural networks for Hamiltonian systems. *Journal of Computational Physics*, 521:113536, 2024. doi:10.1016/j.jcp.2024.113536.
- [21] Peter Benner, Mario Ohlberger, Albert Cohen, and Karen Willcox. *Model reduction and approximation: theory and algorithms*. SIAM, 2017. doi:10.1137/1.9781611974829.
- [22] Peter Benner, Wil Schilders, Stefano Grivet-Talocia, Alfio Quarteroni, Gianluigi Rozza, and Luís Miguel Silveira. *Model Order Reduction: Volume 2: Snapshot-Based Methods and Algorithms*. De Gruyter, 2020. doi:10.1515/9783110671490.
- [23] Gabriele Santin and Bernard Haasdonk. Kernel methods for surrogate modeling. In *Model Order Reduction*, volume 2. De Gruyter, 2021. doi:10.1515/9783110498967-009.
- [24] Daniel Wirtz and Bernard Haasdonk. A vectorial kernel orthogonal greedy algorithm. *Dolomites Research Notes on Approximation*, 6:83–100, 2013. doi:10.14658/PUPJ-DRNA-2013-Special_Issue-10.
- [25] Junbin Gao, Paul W. Kwan, and Daming Shi. Sparse kernel learning with LASSO and Bayesian inference algorithm. *Neural Networks*, 23(2):257–264, 2010. doi:10.1016/j.neunet.2009.07.001.
- [26] Tizian Wenzel, Gabriele Santin, and Bernard Haasdonk. Analysis of target data-dependent greedy kernel algorithms: Convergence rates for f -, $f \cdot P$ - and f/P -greedy. *Constructive Approximation*, 57(1):45–74, 2023. doi:10.1007/s00365-022-09592-3.
- [27] Gabriele Santin, Dominik Wittwar, and Bernard Haasdonk. Greedy regularized kernel interpolation. *preprint arXiv:1807.09575*, 2018. doi:10.48550/arXiv.1807.09575.
- [28] Gabriele Santin, Tizian Wenzel, and Bernard Haasdonk. On the optimality of target-data-dependent kernel greedy interpolation in Sobolev reproducing kernel Hilbert spaces. *SIAM Journal on Numerical Analysis*, 62(5):2249–2275, 2024. doi:10.1137/23M1587956.
- [29] Robert Schaback. A greedy method for solving classes of PDE problems. *preprint arXiv:1903.11536*, 2019. doi:10.48550/arXiv.1903.11536.
- [30] Kristof Albrecht and Armin Iske. On the convergence of generalized kernel-based interpolation by greedy data selection algorithms. *BIT Numerical Mathematics*, 65(1):5, 2025. doi:10.1007/s10543-024-01048-3.
- [31] Tizian Wenzel, Daniel Winkle, Gabriele Santin, and Bernard Haasdonk. Adaptive meshfree approximation for linear elliptic partial differential equations with PDE-greedy kernel methods. *BIT Numerical Mathematics*, 65(1):11, 2025. doi:10.1007/s10543-025-01053-0.
- [32] Douglas Cline. *Variational principles in classical mechanics*. University of Rochester River Campus Librarie, 2017.
- [33] Ernst Hairer and Christian Lubich. Numerical solution of ordinary differential equations. *The Princeton companion to applied mathematics*, pages 293–305, 2012.

- [34] Monique Chyba, Ernst Hairer, and Gilles Vilmart. The role of symplectic integrators in optimal control. *Optimal control applications and methods*, 30(4):367–382, 2009.
- [35] Iharka Csillik. Symplectic and regularization methods. *Technische Mechanik-European Journal of Engineering Mechanics*, 24(1):67–73, 2004.
- [36] Liqian Peng and Kamran Mohseni. Symplectic Model Reduction of Hamiltonian Systems. *SIAM Journal on Scientific Computing*, 38(1):A1–A27, 2016. doi:10.1016/j.cma.2023.116402.
- [37] Patrick Buchfink, Ashish Bhatt, and Bernard Haasdonk. Symplectic Model Order Reduction with Non-Orthonormal Bases. *Mathematical and Computational Applications*, 24(2), 2019. ISSN 2297-8747. doi:10.3390/mca24020043.
- [38] Babak Maboudi Afkham and Jan S. Hesthaven. Structure preserving model reduction of parametric Hamiltonian systems. *SIAM Journal on Scientific Computing*, 39(6):A2616–A2644, 2017. doi:10.1137/17M1111991.

Appendix

First, we focus on how the point-wise derivative error can be bounded by the derivative power function and the error in the RKHS norm.

Lemma 1 (Power-function control via (6)). *For every $m \geq 0$, $x \in \Omega$, and $\ell \in \mathcal{J}$,*

$$|\partial_\ell e_m(x)| = |\langle e_m, (I - \Pi_m) \partial_\ell^{(2)} k(\cdot, x) \rangle_{H_k(\Omega)}| \leq \|e_m\|_{H_k(\Omega)} P_m(x, \ell).$$

Consequently, $\max_{\ell \in \mathcal{J}} \sup_{x \in \Omega} |\partial_\ell e_m(x)| \leq \|e_m\|_{H_k(\Omega)} \sup_{x, \ell} P_m(x, \ell)$.

Proof. By the reproducing property (6),

$$\partial_\ell e_m(x) = \langle e_m, \partial_\ell^{(2)} k(\cdot, x) \rangle_{H_k(\Omega)}.$$

Let $V_m = \text{span}\{\partial_{\ell_i}^{(2)} k(\cdot, x_i) : i = 1, \dots, m\}$ and let Π_m be the orthogonal projector onto V_m . Since $s_m = \Pi_m u$, we have $e_m = u - s_m = (I - \Pi_m)u$, hence $e_m \perp V_m$ and in particular

$$\langle e_m, \Pi_m \partial_\ell^{(2)} k(\cdot, x) \rangle_{H_k(\Omega)} = 0.$$

Therefore,

$$\partial_\ell e_m(x) = \langle e_m, \partial_\ell^{(2)} k(\cdot, x) \rangle_{H_k(\Omega)} = \langle e_m, (I - \Pi_m) \partial_\ell^{(2)} k(\cdot, x) \rangle_{H_k(\Omega)}.$$

Taking absolute values and using Cauchy–Schwarz,

$$|\partial_\ell e_m(x)| = |\langle e_m, (I - \Pi_m) \partial_\ell^{(2)} k(\cdot, x) \rangle_{H_k(\Omega)}| \leq \|e_m\|_{H_k(\Omega)} \|(I - \Pi_m) \partial_\ell^{(2)} k(\cdot, x)\|_{H_k(\Omega)}.$$

By definition of the power function, $P_m(x, \ell) := \|(I - \Pi_m) \partial_\ell^{(2)} k(\cdot, x)\|_{H_k(\Omega)}$, which gives the claimed inequality. Maximizing over $x \in \Omega$ and $\ell \in \mathcal{J}$ yields

$$\max_{\ell \in \mathcal{J}} \sup_{x \in \Omega} |\partial_\ell e_m(x)| \leq \|e_m\|_{H_k(\Omega)} \sup_{\ell \in \mathcal{J}} \sup_{x \in \Omega} P_m(x, \ell).$$

□

Next, we focus on quantifying the error decay in the RKHS norm.

Lemma 2 (Orthogonal update and projection error). *Let*

$$a_m := |\partial_{\ell_{m+1}} e_m(x_{m+1})| = |\langle e_m, (I - \Pi_m) \partial_{\ell_{m+1}}^{(2)} k(\cdot, x_{m+1}) \rangle_{H_k(\Omega)}|, \quad (16)$$

$$b_m := P_m(x_{m+1}, \ell_{m+1}) = \|(I - \Pi_m) \partial_{\ell_{m+1}}^{(2)} k(\cdot, x_{m+1})\|. \quad (17)$$

Then

$$s_{m+1} = s_m + \frac{\langle e_m, (I - \Pi_m) \partial_{\ell_{m+1}}^{(2)} k(\cdot, x_{m+1}) \rangle_{H_k(\Omega)}}{b_m^2} \left((I - \Pi_m) \partial_{\ell_{m+1}}^{(2)} k(\cdot, x_{m+1}) \right),$$

$$\|e_{m+1}\|_{H_k(\Omega)}^2 = \|e_m\|_{H_k(\Omega)}^2 - \frac{a_m^2}{b_m^2}.$$

(We adopt the convention that if $b_i = 0$ which implies $a_i = 0$, the fraction is 0.)

Proof. Recall $V_m = \text{span}\{\partial_{\ell_i}^{(2)} k(\cdot, x_i) : i = 1, \dots, m\}$ and that $s_m = \Pi_m u$ is the orthogonal projector of u onto V_m , so $e_m = u - s_m = (I - \Pi_m)u$ and $e_m \perp V_m$. Put

$$w_m := (I - \Pi_m) \partial_{\ell_{m+1}}^{(2)} k(\cdot, x_{m+1}) \in H_k(\Omega).$$

Since Π_m is an orthogonal projector ($\Pi_m = \Pi_m^*$ and $\Pi_m^2 = \Pi_m$), for any $v \in V_m$ we have $\Pi_m v = v$ and hence

$$\begin{aligned} \langle w_m, v \rangle_{H_k(\Omega)} &= \langle \partial_{\ell_{m+1}}^{(2)} k(\cdot, x_{m+1}) - \Pi_m \partial_{\ell_{m+1}}^{(2)} k(\cdot, x_{m+1}), v \rangle_{H_k(\Omega)} \\ &= \langle \partial_{\ell_{m+1}}^{(2)} k(\cdot, x_{m+1}), v \rangle_{H_k(\Omega)} - \langle \partial_{\ell_{m+1}}^{(2)} k(\cdot, x_{m+1}), \Pi_m v \rangle_{H_k(\Omega)} \\ &= 0. \end{aligned}$$

Thus $w_m \perp V_m$ and therefore

$$V_{m+1} = V_m \oplus \text{span}\{w_m\}$$

is an orthogonal direct sum.

If $b_m = \|w_m\|_{H_k(\Omega)} = 0$, then $w_m = 0$, so $V_{m+1} = V_m$, $s_{m+1} = s_m$ and $e_{m+1} = e_m$. In this case $a_m = |\langle e_m, w_m \rangle_{H_k(\Omega)}| = 0$, and both displayed identities hold trivially. Hence we may assume $b_m > 0$ in the remainder.

Because V_{m+1} is an orthogonal sum and s_{m+1} is the orthogonal projection of u onto V_{m+1} , the standard formula for projection onto a one-dimensional orthogonal extension gives

$$s_{m+1} = s_m + \alpha_m w_m, \quad \alpha_m := \frac{\langle u - s_m, w_m \rangle_{H_k(\Omega)}}{\|w_m\|_{H_k(\Omega)}^2} = \frac{\langle e_m, w_m \rangle_{H_k(\Omega)}}{b_m^2}.$$

This yields the asserted update formula for s_{m+1} .

For the projection error identity, compute

$$e_{m+1} = u - s_{m+1} = u - (s_m + \alpha_m w_m) = e_m - \alpha_m w_m.$$

Hence

$$\begin{aligned} \|e_{m+1}\|_{H_k(\Omega)}^2 &= \|e_m - \alpha_m w_m\|_{H_k(\Omega)}^2 = \|e_m\|_{H_k(\Omega)}^2 - 2\alpha_m \langle e_m, w_m \rangle_{H_k(\Omega)} + \alpha_m^2 \|w_m\|_{H_k(\Omega)}^2 \\ &= \|e_m\|_{H_k(\Omega)}^2 - 2 \frac{\langle e_m, w_m \rangle_{H_k(\Omega)}}{\|w_m\|_{H_k(\Omega)}^2} \langle e_m, w_m \rangle_{H_k(\Omega)} + \left(\frac{\langle e_m, w_m \rangle_{H_k(\Omega)}}{\|w_m\|_{H_k(\Omega)}^2} \right)^2 \|w_m\|_{H_k(\Omega)}^2 \\ &= \|e_m\|_{H_k(\Omega)}^2 - \frac{|\langle e_m, w_m \rangle_{H_k(\Omega)}|^2}{\|w_m\|_{H_k(\Omega)}^2} = \|e_m\|_{H_k(\Omega)}^2 - \frac{a_m^2}{b_m^2}, \end{aligned}$$

because $a_m = |\langle e_m, w_m \rangle_{H_k(\Omega)}|$ by definition and $b_m = \|w_m\|_{H_k(\Omega)}$, i.e., $\|e_m\|_{H_k(\Omega)}^2$ is nonincreasing. \square

In the next lemma, we bound the geometric mean of the quotients $|\partial_{\ell_{m+1}} e_m(x_{m+1})|/P_m(x_{m+1}, \ell_{m+1})$ over a block.

Lemma 3. *For any $m \geq 1$,*

$$\left[\prod_{i=m+1}^{2m} \frac{a_i}{b_i} \right]^{1/m} \leq m^{-1/2} \|e_{m+1}\|_{H_k(\Omega)}.$$

Proof. From Lemma 2, for every $i \geq 0$,

$$\|e_{i+1}\|_{H_k(\Omega)}^2 = \|e_i\|_{H_k(\Omega)}^2 - \frac{a_i^2}{b_i^2}.$$

Set $t_i := a_i^2/b_i^2 \geq 0$ for $i = m+1, \dots, 2m$. Summing gives

$$\sum_{i=m+1}^{2m} t_i = \|e_{m+1}\|_{H_k(\Omega)}^2 - \|e_{2m+1}\|_{H_k(\Omega)}^2 \leq \|e_{m+1}\|_{H_k(\Omega)}^2.$$

By the Arithmetic mean–geometric mean (AM–GM) inequality applied to t_{m+1}, \dots, t_{2m} ,

$$\left(\prod_{i=m+1}^{2m} t_i \right)^{1/m} \leq \frac{1}{m} \sum_{i=m+1}^{2m} t_i \leq \frac{\|e_{m+1}\|_{H_k(\Omega)}^2}{m}.$$

Taking square roots yields

$$\left(\prod_{i=m+1}^{2m} \frac{a_i^2}{b_i^2} \right)^{1/(2m)} \leq m^{-1/2} \|e_{m+1}\|_{H_k(\Omega)}.$$

Since $\left(\prod_{i=m+1}^{2m} \frac{a_i^2}{b_i^2} \right)^{1/(2m)} = \left[\prod_{i=m+1}^{2m} \frac{a_i}{b_i} \right]^{1/m}$, the claim follows. If some $b_i = 0$, then $a_i = 0$ and the product on the left is 0, so the inequality is trivial. \square

Next, we combine the three lemmas to finally prove Theorem 1 and bound the geometric mean of the maximum derivative errors, i.e., of $\max_{\ell \in \mathcal{J}} \sup_{x \in \Omega} |\partial_\ell e_i(x)|$.

Proof of Theorem 1. Fix $m \geq 1$ and define a_i, b_i as in Lemma 2.

By Lemma 2, $\|e_{i+1}\|_{H_k(\Omega)}^2 = \|e_i\|_{H_k(\Omega)}^2 - a_i^2/b_i^2 \leq \|e_i\|_{H_k(\Omega)}^2$, hence $\|e_i\|_{H_k(\Omega)} \leq \|e_{m+1}\|_{H_k(\Omega)}$ for all $i \in \{m+1, \dots, 2m\}$. Lemma 3 gives

$$\left(\prod_{i=m+1}^{2m} \frac{a_i}{b_i} \right)^{1/m} \leq m^{-1/2} \|e_{m+1}\|_{H_k(\Omega)}. \quad (18)$$

For each $i \in \{m+1, \dots, 2m\}$, the f -greedy rule picks (x_{i+1}, ℓ_{i+1}) with

$$a_i = |\partial_{\ell_{i+1}} e_i(x_{i+1})| = \max_{\ell \in \mathcal{J}} \sup_{x \in \Omega} |\partial_\ell e_i(x)|.$$

Thus

$$\begin{aligned} \left(\prod_{i=m+1}^{2m} \max_{\ell \in \mathcal{J}} \sup_x |\partial_\ell e_i(x)| \right)^{1/m} &= \left(\prod_{i=m+1}^{2m} a_i \right)^{1/m} = \left(\prod_{i=m+1}^{2m} \frac{a_i}{b_i} \right)^{1/m} \left(\prod_{i=m+1}^{2m} b_i \right)^{1/m} \\ &\leq m^{-1/2} \|e_{m+1}\|_{H_k(\Omega)} \left[\prod_{i=m+1}^{2m} P_i(x_{i+1}, \ell_{i+1}) \right]^{1/m}. \end{aligned} \quad (19)$$

Let $u_i := \max_{\ell \in \mathcal{J}} \sup_{x \in \Omega} |\partial_\ell e_i(x)| \geq 0$. Then

$$\min_{m+1 \leq i \leq 2m} u_i = \left(\prod_{i=m+1}^{2m} \min_{m+1 \leq i \leq 2m} u_i \right)^{1/m} \leq \left(\prod_{i=m+1}^{2m} u_i \right)^{1/m},$$

and thus, by (19),

$$\min_{m+1 \leq i \leq 2m} \max_{\ell \in \mathcal{J}} \sup_{x \in \Omega} |\partial_\ell e_i(x)| \leq m^{-1/2} \|e_{m+1}\|_{H_k(\Omega)} \left[\prod_{i=m+1}^{2m} P_i(x_{i+1}, \ell_{i+1}) \right]^{1/m}.$$

Using

$$\|\nabla e_i(x)\|_2 \leq \sqrt{n} \max_{\ell \in \mathcal{J}} |\partial_\ell e_i(x)| \quad \text{for all } x \in \Omega$$

yields

$$\min_{m+1 \leq i \leq 2m} \|\nabla e_i\|_{L^\infty(\Omega)} \leq \sqrt{n} m^{-1/2} \|e_{m+1}\|_{H_k(\Omega)} \left[\prod_{i=m+1}^{2m} P_i(x_{i+1}, \ell_{i+1}) \right]^{1/m}. \quad (20)$$

□